

Zero Dynamics, Pendulum Models, and Angular Momentum in Feedback Control of Bipedal Locomotion

Yukai Gong and Jessy Grizzle

Abstract—Low-dimensional models are ubiquitous in the bipedal robotics literature. On the one hand is the community of researchers that bases feedback control design on pendulum models selected to capture the center of mass dynamics of the robot during walking. On the other hand is the community that bases feedback control design on virtual constraints, which induce a passive low-dimensional model in the closed-loop system. In the first case, the low-dimensional model is valued for its physical insight and analytical tractability. In the second case, the low-dimensional model is integral to a rigorous analysis of the stability of walking gaits in the full-dimensional model of the robot. *This paper brings these two approaches (communities) together, clarifying their commonalities and differences. In the process of doing so, we argue that angular momentum about the contact point is a better indicator of robot state than linear velocity. Concretely, we show that an approximate (pendulum and zero dynamics) model parameterized by angular momentum provides better predictions for foot placement on a physical robot (e.g., legs with mass) than does a related approximate model parameterized in terms of linear velocity. We implement an associated angular-momentum-based controller on Cassie, a 3D robot, and demonstrate high agility and robustness in experiments.*

Index Terms—Bipedal robots, zero dynamics, pendulum models, angular momentum

I. INTRODUCTION

Models of realistic bipedal robots tend to be high-dimensional, hybrid, nonlinear systems. This paper is concerned with two major themes in the literature for “getting around” the analytical and computational obstructions posed by realistic models of bipeds.

On the one hand are the broadly used, simplified pendulum models [1]–[7] that provide a computationally attractive model for the center of mass dynamics of a robot. When used for control design, the fact that they ignore the remaining dynamics of the robot generally makes it impossible to prove stability properties of the closed-loop system. Despite the lack of analytical backing, the resulting controllers often work in practice when the center of mass is well regulated to match the assumptions underlying the model. Within this context, the dominant low-dimensional pendulum model by far is the so-called linear inverted pendulum model, or LIP model for short, which captures the center of mass dynamics of a real robot correctly when, throughout a step, the following conditions hold: (i) the center of mass (CoM) moves in a straight line; and (ii), the robot’s angular momentum about the center of mass is zero (or constant). This latter condition can be met by

designing a robot to have light legs, such as the Cassie robot by Agility Robotics [8], or by designing slow gaits to mitigate the contributions of heavy legs to angular momentum about the center of mass.

On the other hand, the control-centric approach called the Hybrid Zero Dynamics provides a mathematically-rigorous gait design and stabilization method for realistic bipedal models [9]–[18] without restrictions on robot or gait design. In this approach, the joints of the robot are synchronized via the imposition of “virtual constraints”, meaning the constraints are achieved through the action of a feedback controller instead of contact forces, and moreover, they can be re-programmed on the fly. Imposing the virtual constraints renders a low-dimensional subset of the dynamics unobservable. The term “zero dynamics” for this unobservable dynamics comes from the original work of [19], [20]. The term “hybrid zero dynamics” or HZD comes from the extension of zero dynamics to (hybrid) robot models in [21]. A downside of this approach, however, has been that it lacked the “physical insight” and “analytical tractability” provided by the pendulum models¹, reducing its wider adoption.

In [25], De-León-Gómez et al. introduced the concept of the *essential dynamics* of a fully actuated robot and studied its relations with the 3D LIP model. The essential dynamics is parameterized by the evolution of the “non-controlled (or free) internal state” of the robot and the desired position of the ZMP. Similar to the zero dynamics, it provides an exact representation of the robot’s “centroidal dynamics” and its calculation as a function of the robot’s body coordinates is the

¹The approaches in [22]–[24] to build reduced-order models via embeddings is a step toward attaching physical significance to the variables in the models.



Fig. 1: Cassie Blue, by Agility Robotics, on the iconic University of Michigan Wave Field.

Funding for this work was provided in part by the Toyota Research Institute (TRI) under award number No. 02281 and in part by NSF Award No. 1808051. All opinions are those of the authors.

The authors are with the College of Engineering and the Robotics Institute, University of Michigan, Ann Arbor, MI 48109 USA {ykgong, grizzle}@umich.edu

same as that of the zero dynamics. The main differences with respect to the hybrid zero dynamics are that (1) the essential dynamics is not tied to the zeroing of an output (making it more general, in a certain sense) and (2) a formal stability theory has not yet been developed for it (leaving work to be done).

A. Objectives

The objectives of this paper are two-fold. Firstly, we seek a rapprochement of the most common pendulum models and the hybrid zero dynamics of a bipedal robot in the case of planar robot models. While we suspect that a 3D extension is possible along the lines of the 3D essential dynamics [25] or the VLIP [26] (LIP with vertical oscillations), it is not attempted here, primarily to keep the arguments as transparent as possible; we will make use of the essential dynamics in 2D. Secondly, we seek to contribute insight on how pendulum models relate among one another and to the dynamics of a physical robot. We demonstrate that even when two pendulum models originate from the same (correct) dynamical principles (e.g., same essential dynamics), the approximations made in different coordinate representations lead to non-equivalent approximations of the dynamics of a (realistic) bipedal robot.

This latter point leads to an important difference in practice; hence we elaborate a bit more here, with details given in Sect. III. Let's only consider trajectories of a robot where the center of mass height is constant, and therefore, the velocity and acceleration of the center of mass height are both zero. In a realistic robot, the angular momentum about the center of mass, denoted by L_c , contributes to the longitudinal evolution of the center of mass, though it is routinely dropped in the most commonly used pendulum models. Can dropping L_c have a larger effect in one simplified model than another?

In the standard 2D LIP model, the coordinates are taken as the horizontal position and velocity of the center of mass and the time derivative of L_c is dropped from the differential equation for the velocity. It follows that the term being dropped is a high-pass filtered version of L_c , due to the derivative. Moreover, the derivative of L_c is directly affected by the motor torques, which are typically "noisy" (have high variance) in a realistic robot. On the other hand, in a less frequently used representation of a 2D inverted pendulum [15], [27]–[29], the coordinates are taken as angular momentum about the contact point and the horizontal position of the center of mass, and L_c is dropped from the differential equation for the position. In this model, L_c (and not \dot{L}_c) shows up in the second derivative of the angular momentum about the contact point. It follows that variations in L_c are low-pass filtered in the second representation as opposed to high-pass filtered in the first, and thus, speaking intuitively, neglecting L_c should induce less approximation error in the second model. More quantitative results are shown in the main body of the paper.

B. Brief Remarks on the Literature

While maintaining "balance" is a critical problem in bipedal locomotion, how the notion of "balance" is quantified and used in the control design can be very different. A common

approach is to summarize the status of a nonlinear high-dimensional robot model with a few key variables. The most frequently proposed variables as surrogates for "balance" include Center of Mass (COM) Velocity [2], [7], [30]–[38], Capture Point [4], [5], Zero Moment Point [39], [40], and Angular Momentum [15], [27], [28], [41].

This paper is mostly closely related to works that equate "balance" with an asymptotically stable periodic orbit. Within this category, we would include all papers on self-synchronization and self-stabilization [42], [43], [43], most papers on the compass gait biped [44]–[47], many papers on simplified pendulum models as found in the survey [48], and papers that treat virtual constraints or zero dynamics [6], [9], [10], [18], [49]–[54].

C. Summary of Main Contributions

Among the above approaches, this paper limits itself to pendulum models and zero dynamics, with the essential dynamics as a link between them.

- Starting from a common physically correct set of equations for real robots, we sequentially enumerate the approximations made to arrive at various reduced order pendulum models, while in parallel, showing in what sense the pendulum models are approximations to the zero dynamics.
- Several advantages of using angular momentum about the contact point as a key variable to summarize the dynamics of a bipedal robot are discussed and demonstrated.
- By their design, solutions of the zero dynamics are also (exact) solutions of the full-order robot model, while for pendulum models, this is not generally the case. We show how simple ideas from zero dynamics can be used to enhance the ability of reduced-order pendulum to capture the dynamics of the robot they are supposed to model and further support why using angular momentum in a reduced-order model provides a more faithful representation of the dynamics of a real robot than does linear velocity.
- We formulate a foot placement strategy based on a high fidelity, one-step-ahead prediction of angular momentum about the contact point.
- We demonstrate that the resulting controller achieves highly dynamic gaits on a Cassie-series bipedal robot.

The last two contributions were introduced in [55] and are used here to demonstrate the utility of the proposed results.

We will use both Rabbit [56] and Cassie Blue, shown in Fig. 1, to illustrate the developments in the paper. Experiments will be conducted exclusively on Cassie.

Rabbit is a 2D biped with five links, four actuated joints, and a mass of 32 Kg; see Fig. 2. Each leg weighs 10 kg, with 6.8 kg on each thigh and 3.2 kg on each shin. The Cassie robot designed and built by Agility Robotics weighs 32kg. It has 7 deg of freedom on each leg, 5 of which are actuated by motors and 2 are constrained by springs; see Fig. 2. A floating base model of Cassie has 20 degrees of freedom. Each foot of the robot is blade-shaped and provides 5 holonomic constraints when firmly in contact with the ground. Though

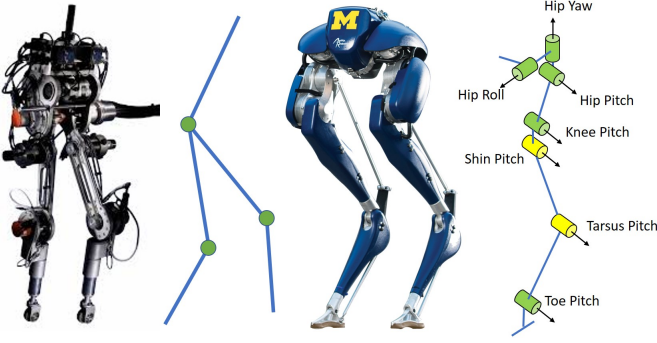


Fig. 2: Rabbit and Cassie. Rabbit is planar robot with 2 joints on each leg and Cassie is 3D robot with 7 joints on each leg.

each of Cassie’s legs has approximately 10 kg of mass, most of the mass is concentrated on the upper part of the leg. In this regard, the mass distribution of Rabbit is more typical of current bipedal robots seen in labs, which is why we include the Rabbit model in the paper.

D. Organization

The remainder of the paper is organized as follows. Section II introduces the full hybrid model of a bipedal robot with instantaneous double support phase. It also summarizes some key properties of the robot’s centroidal dynamics. Section III provides background on a feedback control paradigm based on virtual constraints and the attendant zero dynamics. The essential dynamics are then introduced and presented in various coordinates, and some advantages of models based around angular momentum are highlighted. With this material as background, Sect. IV goes through the approximations made to the essential dynamics in order to arrive at the most popular pendulum models. Because the zero dynamics is obtained from the essential dynamics by evaluating it along trajectories compatible with the virtual constraints, relations between pendulum models and the virtual constraints become manifest, providing three benefits: (1) physical intuition for the zero dynamics; (2) a constructive means to improve the pendulum models; (3) a route to a stability analysis of the full-dimensional closed-loop system. In addition, the effects of making approximations to the zero dynamics and/or essential dynamics in different coordinates are seen. Section V uses a one-step-ahead prediction of angular momentum to decide foot placement. This provides a feedback controller that will stabilize a 3D LIP. In Sect. VI, we provide our path to implementing the controller on Cassie Blue. Additional reference trajectories are required beyond a path for the swing foot, and we provide “an intuitive” method for their design. Section VIII shows the results of experiments. Conclusion are given in Sect. IX.

II. SWING PHASE AND HYBRID MODEL

This section introduces the full-dimensional swing-phase model that describes the mechanical model when the robot is supported on one leg and a hybrid representation used for walking that captures the transition of support legs. The section

concludes with a summary of a few model properties that are ubiquitous when discussing low-dimensional pendulum models of walking.

A. Full-dimensional Single Support Model

We assume a planar bipedal robot satisfying the specific assumptions in [9, Chap. 3.2] and [57], which can be summarized as a passive revolute point contact with the ground, no slipping, all other joints are independently actuated, and all links are rigid and have mass. The gait is assumed to consist of alternating phases of single support (one “foot” on the ground), separated by instantaneous double support phases (both feet in contact with the ground), with the impact between the swing leg and the ground obeying the non-compliant, algebraic contact model in [58], [59] (see also [9, Chap. 3.2]).

We assume a world frame (x, z) with the right-hand rule. We assume the swing-phase (pinned) Lagrangian model is derived in coordinates $q := (q_0, q_1, \dots, q_n) \in Q$, where q_0 is an absolute angle (referenced to the z -axis of the world frame) and $q_b := (q_1, \dots, q_n)$ are body coordinates. Furthermore, we reference the contact point to the origin of the world frame.

With the above sets of assumptions, the robot in single-support has one degree of underactuation and q_0 is a cyclic variable of the kinetic energy. It follows that the dynamic model can be expressed in the form

$$D(q_b)\ddot{q} + C(q, \dot{q})\dot{q} + G(q) = B(q)u, \quad (1)$$

where the vector of motor torques $u \in \mathbb{R}^n$ and the torque distribution matrix has full column rank. The model is written in state space form by defining

$$\begin{aligned} \dot{x} &= \begin{bmatrix} \dot{q} \\ D^{-1}(q_b)[-C(q, \dot{q})\dot{q} - G(q) + B(q)u] \end{bmatrix} \\ &=: f(x) + g(x)u \end{aligned} \quad (2)$$

where $x := (q; \dot{q})$. The state space of the model is $\mathcal{X} = TQ$. For each $x \in \mathcal{X}$, $g(x)$ is a $2(n+1) \times n$ matrix. In natural coordinates $(q; \dot{q})$ for TQ , g is independent of \dot{q} .

B. Hybrid Model

In the above, we implicitly assumed left-right symmetry in the robot so that we could avoid the use of two single-support models—one for each leg playing the role of the stance leg—by relabeling the robot’s coordinates at impact, thereby swapping their roles. Immediately after swapping, the former swing leg is in contact with the ground and is poised to take on the role of the stance leg. The result of the impact and the relabeling of the states provides an expression

$$x^+ = \Delta(x^-) \quad (3)$$

where $x^+ := (q^+; \dot{q}^+)$ (resp. $x^- := (q^-; \dot{q}^-)$) is the state value just after (resp. just before) impact and

$$\Delta(x^-) := \begin{bmatrix} \Delta_q(q^-) \\ \Delta_{\dot{q}}(q^-) \dot{q}^- \end{bmatrix}. \quad (4)$$

A detailed derivation of the impact map is given in [9], showing that it is linear in the generalized velocities.

A hybrid model of walking is obtained by combining the single support model and the impact model to form a system with impulse effects [60]. Even though the mechanical model of the robot is time-invariant, we will allow feedback controllers for (2) that are time varying. So that the hybrid model in closed loop can be analyzed with tools developed for time-invariant hybrid systems, we do the standard “trick” of adding time as a state variable via $\dot{\tau} = 1$. The guard condition (aka switching set) for terminating a step is

$$\mathcal{S} := \{(q, \dot{q}) \in TQ \mid p_{\text{sw}}^z(q) = 0, \dot{p}_{\text{sw}}^z(q, \dot{q}) < 0\}, \quad (5)$$

where $p_{\text{sw}}^z(q)$ is the vertical height of the swing foot. It is noted that \mathcal{S} is independent of time. Combining (2), (3) with the guard set and time gives the hybrid model

$$\Sigma : \begin{cases} \dot{x} = f(x) + g(x)u & x^- \notin \mathcal{S} \\ \dot{\tau} = 1 \\ x^+ = \Delta(x^-) & x^- \in \mathcal{S} \\ \tau^+ = 0. \end{cases} \quad (6)$$

It is emphasized that the guard condition for re-setting the “hybrid time variable”, τ , is determined by foot contact.

C. Swing Phase Model Properties

We conclude this section by summarizing several well-known definitions and properties that will be useful for relating zero dynamics and pendulum models.

- The total mass of the robot is m and g denotes the gravitational constant.
- The position of the center of mass is denoted $p_c = (x_c(q), z_c(q))$. We note that $r_c := \sqrt{x_c^2(q) + z_c^2(q)}$ depends only on q_b .
- The angular momentum about the contact point is denoted L , and due to the choice of coordinates, it can be written as

$$L(q, \dot{q}) = d_0(q_b)\dot{q} = d_{00}(q_b)\dot{q}_0 + d_{0b}(q_b)\dot{q}_b, \quad (7)$$

where $d_0(q_b) = [d_{0a}(q_b), d_{0b}(q_b)]$ is the first row of the mass-inertia matrix $D(q_b)$, partitioned conformally with $q = [q_a; q_b]$. Because $D(q_b)$ is positive definite, $d_{0a}(q_b) > 0$ by standard results on Schur complements.

- The angular momentum about the contact point satisfies

$$\dot{L} = -\frac{\partial V(q)}{\partial q_0}, \quad (8)$$

which shows that L has relative degree three (meaning it must be differentiated three times before the input torques appear [19]). For later use, we note that (8) can also be written as

$$\dot{L} = mgx_c(q). \quad (9)$$

- If L_c denotes the angular momentum about the center of mass, then, by *angular momentum transfer formula*

$$L - L_c = m \begin{bmatrix} x_c \\ z_c \end{bmatrix} \wedge \begin{bmatrix} \dot{x}_c \\ \dot{z}_c \end{bmatrix} = mz_c\dot{x}_c - mx_c\dot{z}_c, \quad (10)$$

where

$$\begin{bmatrix} x_c \\ z_c \end{bmatrix} \wedge \begin{bmatrix} \dot{x}_c \\ \dot{z}_c \end{bmatrix} := \left(\begin{bmatrix} x_c \\ 0 \\ z_c \end{bmatrix} \times \begin{bmatrix} \dot{x}_c \\ 0 \\ \dot{z}_c \end{bmatrix} \right) \cdot \begin{bmatrix} 0 \\ 1 \\ 0 \end{bmatrix}.$$

- If $z_c \equiv H > 0$, a constant, then (10) is typically written as

$$L - L_c = mz_c\dot{x}_c = mHv_c^x, \quad (11)$$

where $v_c := \dot{x}_c$.

- Upon defining $\theta_c := \text{atan}(x_c/z_c)$, the chain rule and (10) result in

$$\dot{\theta}_c = \frac{L - L_c}{mr_c^2(q_b)}. \quad (12)$$

III. CLOSED-LOOP CONTROL, SWING-PHASE ZERO DYNAMICS, AND ESSENTIAL DYNAMICS

Virtual constraints are relations (i.e., constraints) on the state variables of a robot’s model that are achieved through the action of actuators and feedback control instead of physical contact forces. They are called *virtual* because they can be re-programmed on the fly without modifying any physical connections among the links of the robot or its environment. Like physical constraints, under certain regularity conditions², virtual constraints induce a low-dimensional invariant model, called the *zero dynamics*, due to the highly influential paper [20].

The design of virtual constraints, their imposition by feedback control, and the computation of the hybrid zero dynamics have been studied in numerous papers. Here we simply sketch the basic formalism for the swing-phase of the robot model, with a bit more background on the hybrid zero dynamics given in the Appendix. Because our real goal is to establish connections between common pendulum models and the zero dynamics, or approximations of the zero dynamics, we will need to back up one step before the virtual constraints are actually enforced or achieved (depending on one’s point of view) via feedback control. This literally corresponds to looking at the evolution of the robot’s states before they have converged to the zero dynamics manifold. While we would love to dub the differential equations for the zero dynamics in this off-manifold state as the *off-zero dynamics*, they have been named the *essential dynamics* in [25].

A. Virtual Constraints and a Convenient Continuous-time Control Law

We pose the virtual constraints as an output zeroing problem of the form³

$$y = h(q, L, \tau), \quad (13)$$

where h is at least twice continuously differentiable and τ captures time dependence. It is assumed that the decoupling matrix

$$A(q) := \frac{\partial h(q, L, t)}{\partial q} D^{-1}(q_b) B(q) \quad (14)$$

²The regularity conditions refer to (14) being invertible and (18) being injective.

³We design h to have relative degree two, the same as q . We therefore use L instead of \dot{q} because L has relative degree three while \dot{q} has relative degree one. Hence, the relative degree is determined by q .

is invertible on an open neighborhood of the robot's state space. Moreover, it is assumed that $y = h(q, L, \tau)$ is designed to identically vanish on a desired solution (gait) $(\bar{q}(t), \dot{\bar{q}}(t), \bar{u}(t))$ of the dynamical model (6) with $\tau(t) = t$, and that the solution $(\bar{q}(t), \dot{\bar{q}}(t), \bar{u}(t))$ meets relevant constraints on motor torque, motor power, ground reaction forces, and work space. To be clear, y vanishing means

$$h(\bar{q}(t), \bar{L}(t), t) \equiv 0 \quad (15)$$

for $0 \leq t \leq T$, where $\bar{L}(t)$ is the angular momentum about the contact point, evaluated along the trajectory.

For definiteness, a passivity-based input-output (exponentially) stabilizing control law [61]

$$u = \gamma(q, \dot{q}, \tau) \quad (16)$$

is assumed, such that, in closed loop,

$$\hat{D}(\tau)\ddot{y}(\tau) + (\hat{C}(\tau) + K_d)\dot{y}(\tau) + K_p y(\tau) = 0 \quad (17)$$

for some $\hat{D}(\tau)$ strictly positive definite,

$$\hat{D}(\tau) = \hat{C}(\tau) + \hat{C}^\top(\tau),$$

and $K_d > 0$ and $K_p > 0$ positive definite. Details are given in the Appendix. Alternatively, one could use a QP-CLF controller to drive the virtual constraints to zero at a sufficiently rapid exponential rate [62]; other controllers are given in [9].

B. Zero Dynamics

From [20], [63] and [9, Chap. 5], it is known that a feedback achieving (17) necessarily renders part of the closed-loop system “unobservable” through the output y . Moreover, from [63] or [9, Chap. 5],

- for any function $\xi_1(q)$ for which

$$\begin{bmatrix} h(q, L, \tau) \\ \xi_1(q) \\ \tau \end{bmatrix} \quad (18)$$

is injective on the subset of states, where the decoupling matrix is invertible,

- and for $\xi_2 := \dot{\xi}_1$ as well as for $\xi_2 := L$, the set of solutions of the model compatible with the output y being identically zero can be expressed in the form

$$\begin{aligned} q &= \beta_q(\xi_1, \xi_2, \tau) \\ \dot{q} &= \beta_{\dot{q}}(\xi_1, \xi_2, \tau) \\ u &= \alpha(\xi_1, \xi_2, \tau). \end{aligned} \quad (19)$$

The zero dynamics manifold is then the three-dimensional⁴ surface

$$Z := \{(q, \dot{q}, \tau) \in TQ \times \mathbb{R} \mid [q; \dot{q}] = \beta(\xi_1, \xi_2, \tau), 0 \leq \tau \leq T\} \quad (20)$$

contained in $TQ \times \mathbb{R}$. The (hybrid) zero dynamics is then the restriction of the closed-loop hybrid dynamics to Z . In Sec. III-C, we will consider three specific sets of coordinates.

⁴The two state variables ξ_1, ξ_2 and the hybrid time variable τ .

Some readers may wish to take a quick look and then return for the general picture.

Remaining at a general choice of coordinates ξ_1, ξ_2 , one first computes the time derivatives

$$\begin{aligned} \dot{\xi}_1 &:= \frac{\partial \xi_1}{\partial q} \dot{q} \\ \dot{\xi}_2 &:= \frac{\partial \xi_2}{\partial q} \dot{q} + \frac{\partial \xi_2}{\partial \dot{q}} \ddot{q} \\ \dot{\tau} &:= 1. \end{aligned} \quad (21)$$

The second step is to evaluate the terms in (21) using the dynamical model (2) and (19). The result is a three-dimensional autonomous system of the form

$$\begin{bmatrix} \dot{\xi}_1 \\ \dot{\xi}_2 \\ \dot{\tau} \end{bmatrix} = f_{\text{zero}}(\xi_1, \xi_2, \tau), \quad (22)$$

called the *swing-phase zero dynamics*.

In applications [9], [11], [27], [31], [33], [64]–[66], it is often convenient to define the virtual constraints via an output of the form

$$y = h(q) =: q_b - h_d(q_0, L, \tau), \quad (23)$$

instead of the more general form (13). If we take $\xi_1 := q_0$ and $\xi_2 := L$, then (7) gives that the unobservable dynamics, which also corresponds to the essential dynamics of [25], can be written as

$$\begin{aligned} \dot{q}_0 &= \frac{L}{d_{00}(q_b)} - \frac{d_{0b}(q_b)}{d_{00}(q_b)} \dot{q}_b \\ \dot{L} &= mgx_c(q_0, q_b), \end{aligned} \quad (24)$$

that is,

$$\begin{aligned} \dot{\xi}_1 &= \frac{\xi_2}{d_{00}(q_b)} - \frac{d_{0b}(q_b)}{d_{00}(q_b)} \dot{q}_b \\ \dot{\xi}_2 &= mgx_c(\xi_1, q_b). \end{aligned} \quad (25)$$

From (23), $y \equiv 0$ gives

$$\begin{aligned} q_b &= h_d(q_0, L, \tau) \\ &= h_d(\xi_1, \xi_2, \tau) \\ \dot{q}_b &= \frac{\partial h_d(q_0, L, \tau)}{\partial q_0} \dot{q}_0 + \frac{\partial h_d(q_0, L, \tau)}{\partial \tau} + \\ &\quad + \frac{\partial h_d(q_0, L, \tau)}{\partial L} mgx_c(q_0, q_b) \\ &= \frac{\partial h_d(\xi_1, \xi_2, \tau)}{\partial \xi_1} \dot{\xi}_1 + \frac{\partial h_d(\xi_1, \xi_2, \tau)}{\partial \tau} + \\ &\quad + \frac{\partial h_d(\xi_1, \xi_2, \tau)}{\partial \xi_2} mgx_c(\xi_1, h_d(\xi_1, \xi_2, \tau)) \end{aligned} \quad (26)$$

Substituting (26) into (25) gives the swing-phase zero dynamics

$$\begin{aligned} \dot{\xi}_1 &= \frac{\xi_2 - \kappa_1(\xi_1, \xi_2, \tau)}{\kappa_2(\xi_1, \xi_2, \tau)} \\ \dot{\xi}_2 &= \kappa_3(\xi_1, \xi_2, \tau) \\ \dot{\tau} &= 1, \end{aligned} \quad (27)$$

where, dropping arguments for reasons of space,

$$\begin{bmatrix} \kappa_1(\xi_1, \xi_2, \tau) \\ \kappa_2(\xi_1, \xi_2, \tau) \\ \kappa_3(\xi_1, \xi_2, \tau) \end{bmatrix} := \begin{bmatrix} d_{0b} \frac{\partial h_d}{\partial \xi_2} mgx_c - \frac{\partial h_d}{\partial \tau} \\ d_{00} + d_{0b} \frac{\partial h_d}{\partial \xi_1} \\ mgx_c \end{bmatrix}, \quad (26)$$

that is, all terms are evaluated at (26). Moreover, from [19], $\kappa_2 \neq 0$ everywhere the decoupling matrix is invertible.

C. Essential or Unobservable Dynamics in other Coordinates

Equations (24) and (27) are pendulum models, of a sort, but they are hard to interpret. Later, we'll see that κ_1 may roughly be thought of as the "angular momentum about the center of mass", κ_2 is roughly an "inertia", while we know that κ_3 is the torque exerted by gravity about the contact point.

In the following, we provide the essential dynamics for three additional sets of coordinates (ξ_1, ξ_2)

- (x_c, v_c^x)
- (x_c, L) , and
- (θ_c, L) ,

and will then dedicate Sect. IV to establishing connections between pendulum models and zero dynamics that are more easily/intuitively grounded in physics.

Case 1: $(\xi_1 = x_c, \xi_2 = v_c^x)$ **Horizontal Position and Velocity** Differentiating (10) and using $v_c = \dot{x}_c$ results in

$$\begin{aligned} \dot{x}_c &= v_c^x \\ \dot{v}_c &= \frac{g}{z_c} x_c + \frac{\ddot{z}_c}{z_c} x_c - \frac{\dot{L}_c}{m z_c}, \end{aligned} \quad (28)$$

In general z_c depends on q , \dot{z}_c depends on both q and \dot{q} , L_c depends on q_b and \dot{q}_b . While \dot{L}_c and \ddot{z}_c depend on q , \dot{q} , and the motor torques u , it is more typical to use the ground reaction forces. In particular, one uses $\ddot{z} = g - \frac{1}{m} F_z$ and $\dot{L}_c := \frac{d}{dt} L_c = x_c F_z - z_c F_x$, where F_x and F_z are the horizontal and vertical components of the ground reaction forces. In turn, the ground reaction forces can be expressed as functions of q , \dot{q} , and the motor torques, u .

Case 2: $(\xi_1 = x_c, \xi_2 = L)$ **Angular Momentum and Horizontal Position:** Differentiating (10) and using (9) results in

$$\begin{aligned} \dot{x}_c &= \frac{L - L_c}{m z_c} + \frac{\dot{z}_c}{z_c} x_c \\ \dot{L} &= m g x_c. \end{aligned} \quad (29)$$

The remarks made above on z_c , \dot{z}_c , and L_c apply here as well.

Case 3: $(\xi_1 = \theta_c, \xi_2 = L)$ **Alternative absolute angle (cyclic variable):** Combining (9) and (12) yields

$$\begin{aligned} \dot{\theta}_c &= \frac{L - L_c}{m r_c^2} \\ \dot{L} &= m g r_c \sin(\theta_c). \end{aligned} \quad (30)$$

In comparison to (24), it's now easier to interpret the way in which the actuated states enter the dynamics, namely, through r_c , the length of a pendulum representation of the center of mass, and L_c , the angular momentum about the center of mass. It is remarkable that the derivatives of the actuated states only appear through L_c .

Remark: It can be shown that θ_c is a cyclic variable and hence (24) holds. It follows that when $q_0 = \theta_c$,

$$\begin{aligned} d_{00}(q_b) &= m r_c^2, \text{ and} \\ d_{0b}(q_b) \dot{q}_b &= L_c. \end{aligned} \quad (31)$$

For some of the control designs in [9], the absolute angle q_0 was taken as the angle of the line from the contact point to the

robot's hip, which is a rough approximation of the angle θ_c . The extent to which the relations in (31) hold approximately was never investigated. In the well known LIP model, L_c is treated as negligible and dropped. We'll argue later for keeping it so that robots with "heavy legs" (i.e., legs with non-negligible mass) can be better accommodated. Nevertheless, dropping $d_{0b}(q_b) \dot{q}_b$ in (24) yields the simpler, approximate model

$$\begin{aligned} \dot{q}_0 &= \frac{L}{d_{00}(q_b)} \\ \dot{L} &= m g x_c(q_0, q_b) \end{aligned} \quad (32)$$

for the observable dynamics, and ultimately, as we will see in the next Section, for the zero dynamics as well.

D. Angular Momentum about Contact Point

In this paper, we are focusing on the angular momentum about the contact point, L , as a replacement of the center of mass velocity, v_c , which is used as an indicator of walking status in many other papers [7], [18], [32], [67]. Specific to this paper, L is also a state of the zero dynamics. Before we proceed to that, it is beneficial to explain why L can replace v_c , summarize some general properties of L , and highlight some of its advantages versus v_c . More specific advantages of using L in the zero dynamics and the LIP model will be discussed in later sections.

We first need to answer why L can replace v_c as an indicator of walking. The relationship between angular momentum and **linear momentum** for a 3D bipedal robot is

$$L = L_c + p_c \wedge m v_c, \quad (33)$$

where L_c is the angular momentum about the center of mass, v_c is the linear velocity of the center of mass, m is the total mass of the robot, and p_c is the vector emanating from the contact point to the center of mass.

For a bipedal robot that is walking instead of doing somersaults, it is reasonable to focus on gaits where the angular momentum about the center of mass must oscillate about zero (e.g., arms are not rotating as in a flywheel). When this is true, (33) implies that the difference between L and $p_c \wedge m v_c$ also oscillates around zero, which we will write as

$$L - p_c \wedge m v_c = L_c \text{ oscillates about 0.} \quad (34)$$

From (34), we see that we approximately obtain a desired linear velocity by regulating L . Hence, one can replace the control of linear velocity with control of angular momentum about the contact point.

What are there advantages to using L ?

- The first advantage of controlling L is that it provides a more comprehensive representation of current walking status because it is the sum of angular momentum about the center of mass, L_c , and linear momentum, $p_c \wedge m v_c$. From (28) we can see that there exists momentum transfer between these two quantities. If L_c increases, it must "take" some momentum away from v_c , and vice versa [68]. By the nature of walking, unless a flywheel is installed on the robot, L_c must oscillate about zero during a normal step for otherwise, some joints

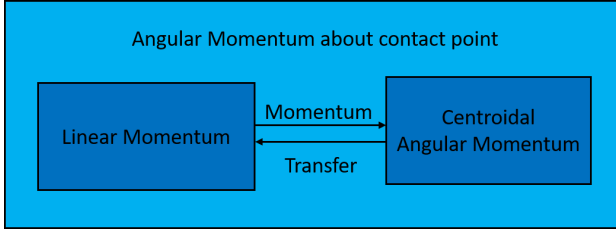


Fig. 3: The relation between L , L_c , and v_c^x . Equation (33) shows L is the sum of L_c and a term that is linear in v_c , while the second line of (24) shows the transfer of momentum between L_c and v_c .

will likely hit their joint limit. L_c functions to store momentum, but importantly it can only store it for a short amount of time. When designing a foot placement strategy, it is better to take the “stored” momentum into account. When balancing on one foot for example, some researchers plan L_c and v_c separately [69], or use L_c as an input to regulate balance by waving the torso, arms, the swing leg [70], [71] or even a flywheel [72]. Here, instead of moving limbs to generate a certain value of L_c , we view L_c as a result of the legs and torso moving to fulfill other tasks. We only observe L_c and take it into consideration through L , and do not design it as an input.

- (b) Secondly, because $\dot{L} = mgx_c$ depends only on the CoM position, it follows that L has relative degree three when ankle torque is omitted. Consequently, the evolution L is weakly affected by joint motor torques during a step. In Fig. 4 (a) and (d) and Fig. 5 (a) we see that the trajectory of L consistently has a convex shape, irrespective of model or speed. We’ll see later the same property in experimental data.
- (c) The discussion so far has focused on the single support phase of a walking gait. Bipedal walking is characterized by the transition between left and right legs as they alternately take on the role of stance leg (aka support leg) and swing leg (aka non-stance leg). In double support, the transfer of angular momentum between the two contact points satisfies

$$L_2 = L_1 + p_{2 \rightarrow 1} \wedge mv_c. \quad (35)$$

Hence, the change of angular momentum between two contact points depends only on the vector defined by the two contact points and the center of mass velocity. In particular, angular momentum about a given contact point is invariant under the impulsive force generated at that new contact point. Consequently, we can easily determine the angular momentum about the new contact point by (35) when impact happens without resorting to approximating assumptions about the impact model. Moreover, if \dot{z}_c is zero and the ground is level, then $p_{2 \rightarrow 1} \wedge mv_c = 0$, and hence $L_2 = L_1$.

Figure 4 shows the evolution of L , v_c^x , L_c and \dot{L}_c during a step for both Cassie and Rabbit, when walking speed is about

2 m/s and $v_c^z = 0$. Figure 5 shows the evolution of L , v_c^x , L_c for Rabbit walking at a range of speeds from -1.8 m/s to 2.0 m/s. We note that the trajectory of L has a consistent convex shape across different robots and speeds, because of $\dot{L} = mgx_c$. Figure 4 and 5 also show the continuity property of L at impact.

E. Impact Model for the Hybrid Zero Dynamics

Substituting (19) or (26) into (4) results in the impact model for the zero dynamics

$$\begin{bmatrix} \xi_1^+ \\ \xi_2^+ \end{bmatrix} = \Delta_{\text{zero}}(\xi_1^-, \xi_2^-). \quad (36)$$

When $\xi_1 = x_c$,

$$\xi_1^+ = p_{\text{sw} \rightarrow \text{CoM}}^{x,-}, \quad (37)$$

the horizontal position of the swing foot relative to the center of mass at the end of a step. For $\xi_1 = \theta_c$, it would be the corresponding angle of the swing leg at the end of the step. Equation (35) gives that for $\xi_2 = L$, the second row of δ_{zero} is simply

$$\xi_2^+ = L^- + p_{\text{sw} \rightarrow \text{st}}^- \wedge mv_c. \quad (38)$$

For $\xi_2 = v_c^x$, the mapping can be derived as in [9], [11]. We do not give details because the prevailing practice in the pendulum community is to assume conditions such that $v_c^+ = v_c^-$.

Though we do not emphasize it here, the behaviour of the y -dynamics (17) under the impact map is also important. This is treated extensively in [18], [73]–[76].

IV. PENDULUM MODELS AND ZERO DYNAMICS

Each of the representations of the essential dynamics in (24), (28), (29), and (30) is valid along all trajectories of the full-dimensional model. Moreover, the zero dynamics of the closed-loop system can be obtained by evaluating any one of them at the corresponding version of (19) or (26), which gives the solutions of the full-dimensional model that are compatible with the virtual constraints being satisfied. This section systematically goes through the models in Sec. III-C and looks for connections with low-dimensional pendulum models, and subsequently, connections between zero dynamics and pendulum models.

A. Constant Pendulum Height

We suppose one component of the virtual constraints in (13) is $z_c(q) - H$, where H is a constant. Then $y \equiv 0$ yields $z_c = H$, $\dot{z}_c = 0$, and $\ddot{z}_c = 0$, simplifying (28) and (29) to

$$\begin{aligned} \dot{x}_c &= v_c^x \\ \dot{v}_c^x &= \frac{g}{H} x_c - \frac{\dot{L}_c}{mH}, \end{aligned} \quad (39)$$

and

$$\begin{aligned} \dot{x}_c &= \frac{L}{mH} - \frac{L_c}{mH} \\ \dot{L} &= mgx_c, \end{aligned} \quad (40)$$

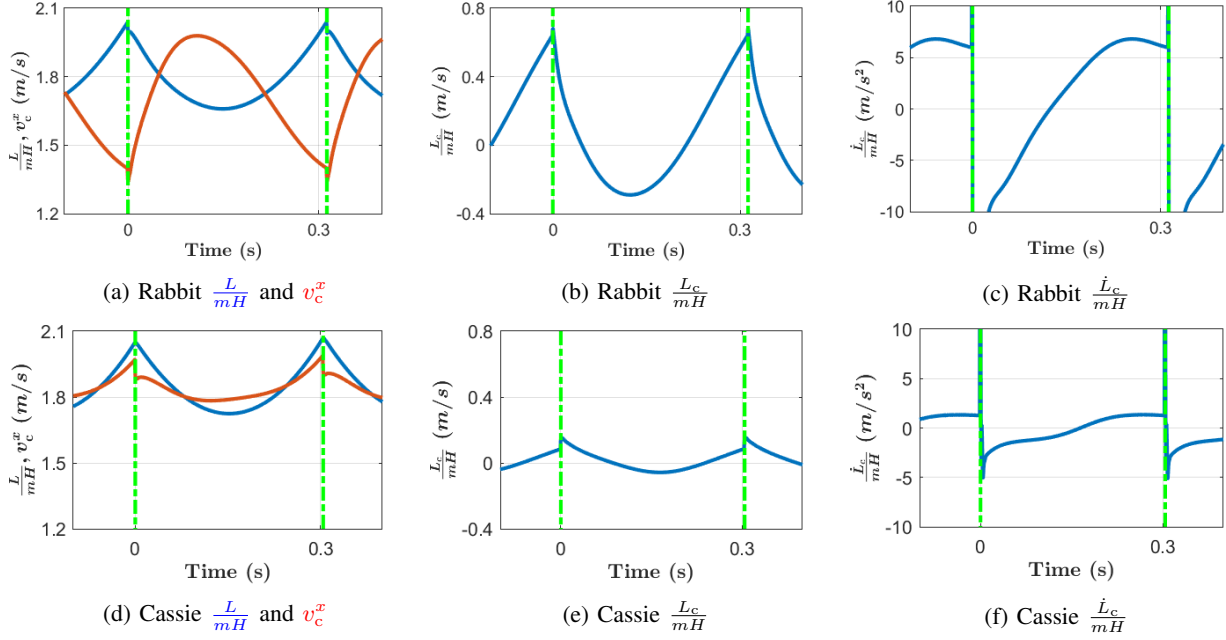


Fig. 4: Plots of L , v_c , and \dot{L}_c for the bipedal robots Rabbit and Cassie walking at about 2m/s, while v_c^z is carefully regulated to zero. The vertical green lines indicate the moment of impact. For both robots, the angular momentum about the contact point, L , has a convex shape, similar to the trajectory of a LIP model, while the trajectory of the longitudinal velocity of the center of mass, v_c^x , has no consistent shape. The variation of L_c throughout a step, which is caused by the legs of the robot having mass, is what leads to a difference in the CoM velocity between a real robot and a LIP model. In this figure, L is continuous at impact, which is based on two conditions: $v_c^z = 0$ at impact and the ground is level. Even when these two conditions are not met, the jump in L at impact can be easily calculated with (35).

respectively. Equation (40) can be rewritten as

$$\begin{aligned} \dot{x}_c &= v_p - \frac{L_c}{mH} \\ \dot{v}_p &= \frac{g}{H} x_c, \end{aligned} \quad (41)$$

where $v_p = \frac{L}{mH}$, which is more directly comparable to (39). In this paper we frequently demonstrate L with a coefficient $\frac{1}{mH}$, so that it could be more directly comparable to v_c .

At this point, no approximations have been made and both models are valid everywhere that $z_c(q) \equiv H$. Hence, the two models are still equivalent when it comes to determining the zero dynamics for any set of virtual constraints that has $z_c(q) - H$ as one of its components. *We'll next argue that the models are not equivalent when it comes to approximations.*

Dropping the \dot{L}_c term in (39) results in:

$$\begin{aligned} \dot{x}_c &= v_c^x \\ \dot{v}_c^x &= \frac{g}{H} x_c. \end{aligned} \quad (42)$$

This is the well-known LIP model proposed by [77].

Dropping L_c in (40) results in

$$\begin{aligned} \dot{x}_c &= \frac{L}{mH} \\ \dot{L} &= mgx_c, \end{aligned} \quad (43)$$

which is used in [28], [29]. To distinguish the model (43) from (42), we will denote it by ALIP, where A stands for Angular Momentum.

For a robot with a point mass, two models (42) and (43) are equivalent. For a real robot with L_c and \dot{L}_c that are nonnegligible, however, we argue that (43) is more accurate than (42) primarily because of three properties,

- Amplitude.** The scale of \dot{L}_c is much larger than L_c over a wide range of velocities; see Figure 4 and 5.
- Relative degree.** L has relative degree two with respect to L_c and three with respect to \dot{L}_c , whereas v_c has relative degree one with respect to \dot{L}_c . This makes v_c much more sensitive to the omission of the L_c term.
- Zero average value.** What makes (43) even more accurate is that L_c oscillates about zero and, moreover, its average value over a step is close to zero, as shown in Table I. Though the data we show here corresponds to the specific controller described in Sec V and VI, we believe it is generally true for other controllers that induce periodic walking. The oscillation of L_c roughly results in the effect of L_c on x_c averaging out to zero over a step. If we seek to predict the value of L with (43) for a longer period of time, the effect of L_c will cancel out because of the oscillation. If we seek to predict L for a shorter time interval, the error will be small because the time duration is short.

In Fig. 6, we have used the models (42) and (43) to predict the values of v_c and L at the end of a step. We plot $\frac{L}{mH}$ instead of L to make the scale and units comparable. The blue line is the true trajectory of L (v_c) during a step. The red

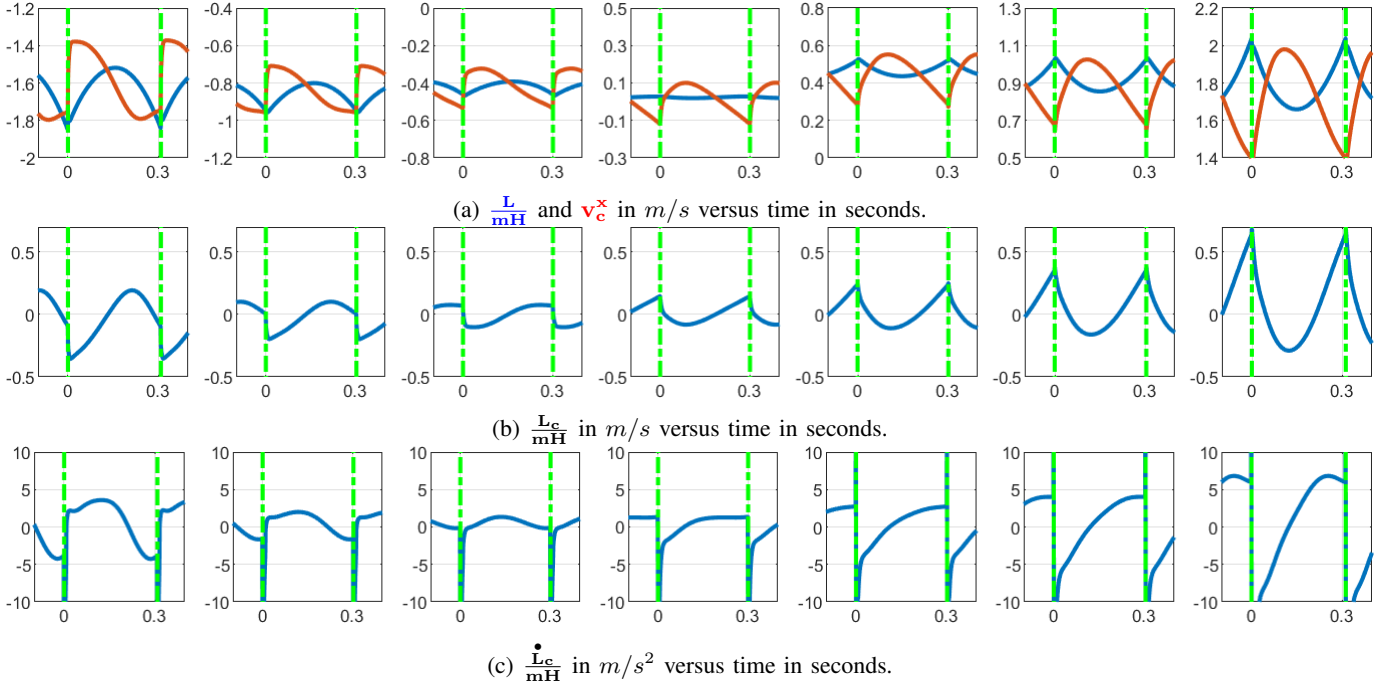


Fig. 5: Plots of L , v_c , and \dot{L}_c for Rabbit walking at different speeds. The green vertical lines indicate the moment of impact. (a) shows that L always has a convex or concave shape like the LIP model, while v_c has no determinant shape. The shape of L is a direct consequence of $\dot{L} = mgx_c$. The quantities $\frac{L}{mH}$ and v_c^x are close in scale and oscillate about one another. This shows that directly regulating L does indeed indirectly regulate v_c . (b) and (c) show the scales of L_c and \dot{L}_c . It is seen that \dot{L}_c is much larger in scale and thus omitting it in (39) can create a larger error than neglecting L_c in (40).

line shows the prediction of L (v_c) at the end of each of step, at each moment throughout a step, based on the instantaneous values of x_c and L (v_c) at that moment. The red line would be perfectly flat if (43) and (42) perfectly captured the evolution of L (v_c), respectively, in the full simulation model, and the flatter the estimate, the more faithful is the representation.

The prediction errors of (42) and (43) caused by neglecting L_c and \dot{L}_c , respectively, are computed to be

$$\begin{aligned} v_e(t_2, t_1) &= e_1(t_2, t_1) \\ &= e_2(t_2, t_1) + e_3(t_2, t_1) \end{aligned} \quad (44)$$

$$\left(\frac{L_e(t_1, t_2)}{mH} \right) = e_2(t_2, t_1), \quad (45)$$

where

$$\begin{aligned} e_1(t_2, t_1) &= -\frac{1}{mH} \int_{t_1}^{t_2} \cosh(\ell(t_2 - \tau)) \dot{L}_c(\tau) d\tau \\ e_2(t_2, t_1) &= -\frac{1}{mH} \int_{t_1}^{t_2} \ell \sinh(\ell(t_2 - \tau)) L_c(\tau) d\tau \\ e_3(t_2, t_1) &= -\frac{1}{mH} (L_c(t_2) - \cosh(\ell(t_2 - t_1)) L_c(t_1)). \end{aligned}$$

Figure 7 shows the (relative) sizes of these error terms. If we view L_c as a disturbance and prediction error as an output, we obtain the corresponding Laplace transforms and Bode plots shown in Fig. 8.

B. Constant Pendulum Length

We suppose one component of the virtual constraints in (13) is $r_c(q) - R$, where R is a constant. Then $y \equiv 0$ yields $r_c = R$,

Speed	-1.60	-0.83	0.02	0.89	1.75
Average L_c	-0.62	-0.27	0.02	0.32	0.74

TABLE I: Average L_c of Rabbit at various walking speeds with a periodic gait.

simplifying (30) to

$$\begin{aligned} \dot{\theta}_c &= \frac{L - L_c}{mR^2} \\ \dot{L} &= mgR \sin(\theta_c). \end{aligned} \quad (46)$$

At this point, no approximations have been made and the models is valid everywhere that $r_c(q) \equiv R$. An interesting aspect of this pendulum model is that it does not depend on \dot{R} , and thus imperfections in achieving the virtual constraint $r_c = R$ have a smaller effect here than in (40), where \dot{z} would appear when $z_c \neq H$, or in (39), where both \dot{z}_c and \ddot{z}_c would appear.

As with (40), the model (46) is driven by the strongly actuated states q_b, \dot{q}_b through L_c and the same discussion applies. Dropping L_c in (29) results in

$$\begin{aligned} \dot{\theta}_c &= \frac{L}{mR^2} \\ \dot{L} &= mgR \sin(\theta_c), \end{aligned} \quad (47)$$

which is nonlinear in θ_c . However, for $R = 1$ and a step length of 60 cm, $\max \theta_c \approx \pi/6$, and for 70 cm, $\max \theta_c \approx \pi/4$, giving

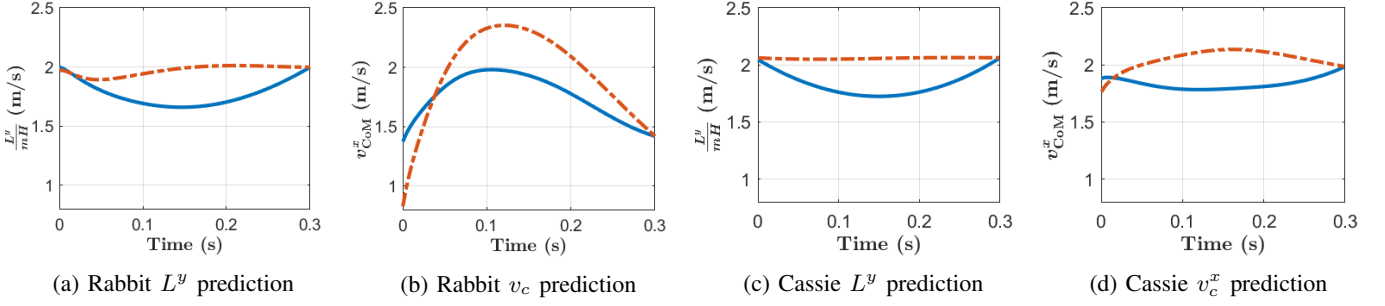


Fig. 6: Comparison of the ability to predict velocity vs angular momentum at the end of a step. The instantaneous values are shown in **blue** and the predicted value at the end of the step is shown in **red**, where a perfect prediction would be a flat line that intercepts the terminal point of the blue line. The most crucial decision in the control of a bipedal robot is where to place the next foot fall. In the standard LIP controller, the decision is based on predicting the longitudinal velocity of the center of mass. In Sect. V we use angular momentum about the contact point. We do this because on realistic bipeds, a LIP-style model provides a more accurate and reliable prediction of L than v_c . The comparison is more significant on Rabbit, whose leg center of mass is further away from the overall center of mass.

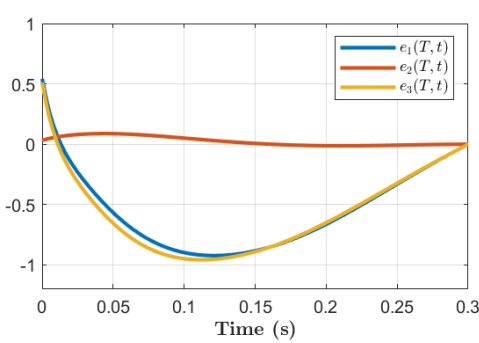


Fig. 7: A plot of the error terms in (44) and (45) resulting from dropping \dot{L}_c and L_c , respectively, for the Rabbit model walking at 2 m/s. The take-home message is that of the terms $e_2(t_1, t_2) + e_3(t_1, t_2)$ in (44) comprising the velocity error of the LIP model, the term $e_3(t_1, t_2)$ shown in the **yellow** line contributes by far the largest portion of the total error shown by the **blue** line. The error of the ALIP model, however, is given only by $e_2(t_1, t_2)$, which results in the significantly reduced prediction error shown by the **red** line.

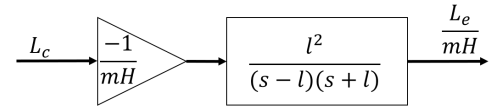
simple bounds on the approximation error,

$$\begin{aligned} \frac{1}{\pi/6} \int_0^{\pi/6} (\theta - \sin(\theta)) d\theta &< 0.006 \\ \frac{1}{\pi/4} \int_0^{\pi/4} (\theta - \sin(\theta)) d\theta &< 0.02. \end{aligned}$$

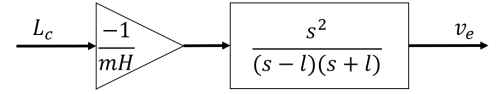
Moreover, if desired, one can chose K to set

$$\frac{1}{\theta_{\max}} \left| \int_0^{\theta_{\max}} (K\theta - \sin(\theta)) d\theta \right| = 0.$$

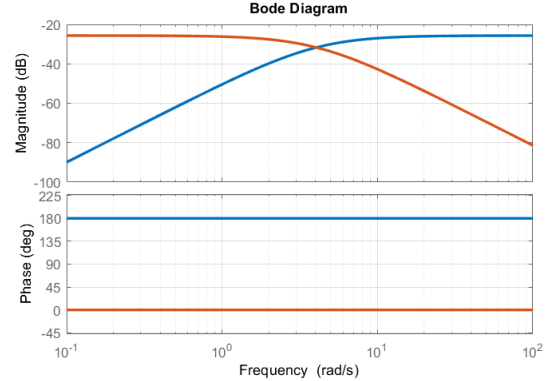
For $\theta_{\max} = \pi/4$, the value is $K \approx 0.95$. While a linear approximation is useful for having a closed-form solution, numerically integrating the nonlinear model (47) in real time is certainly feasible.



(a) ALIPM



(b) LIPM



(c) Bode Plot

Fig. 8: How neglecting L_c and \dot{L}_c generates errors in ALIPM and LIPM. Note the low-pass (ALIPM in **red**) vs high-pass (LIPM in **blue**) nature of the respective transfer functions.

C. Accounting for L_c

The trajectory of L_c is determined by the robot's dynamic model and the movement of its links. In Fig. 5-(b), we observe that L_c has a simple shape⁵. This motivates us to estimate the trajectory of L_c and plug it into (40) to improve our prediction.

For each of a range of walking speeds, we fit the time-based trajectory of L_c during a step with a third-order polynomial in τ . For online use, the four polynomial coefficients in

⁵The trajectories are the result of a controller described in Sect. VI.

$\hat{L}_c(\tau)$ were regressed as second-order polynomials in $L(0)$, the value of L at the beginning of each step. Given the estimate $\hat{L}_c(\tau, L(0))$, we can plug it into (40) and view $\hat{L}_c(\tau, L(0))$ as a time-varying forcing term. Its contribution to predicted angular momentum is then

$$\int_t^T e^{A(T-\tau)} B \hat{L}_c(\tau, L(0)) d\tau, \quad (48)$$

which can be added to an estimate of L . Figure 9 shows the resulting improvements in estimates of scaled angular momentum when Rabbit is walking at various constant speeds. Figure 10 shows that the improvements in estimation persist under transient operation of the robot.

D. Varying Pendulum Length or Center of Mass Height

Varying the pendulum length or the center of mass height is important for traversing slopes or going up/down stairs. Imposing $r_c - R(t)$ as a virtual constraint renders (47) time-varying. While some linear time-varying systems can be integrated in closed form, most cannot. Hence, there is even less reason to pursue a linear approximation of the model. Instead, the low-dimensional nonlinear and/or time-varying model can be numerically integrated in real time or pre-integrated and stored in a table, as discussed for $L_c(t)$.

Imposing $z_c - H(t)$ as a virtual constraint means the \dot{z}_c term from (29) could (should) be retained, and unless $H(t)$ is affine in t , it means the term \ddot{z}_c in (28) could (should) be retained [26].

E. Application to the Zero Dynamics

We emphasize once again that the zero dynamics can be obtained by evaluating any of the essential dynamic models (24), (28), (29), and (30) along the trajectories of the full-dimensional model compatible with the virtual constraints in (19) or (26) being satisfied. For a fixed set of (relative degree two) virtual constraints (with an invertible decoupling matrix), the resulting zero dynamic models are diffeomorphic to one another, meaning they differ by an invertible and differentiable change of coordinates. In particular, they all have the same dimension and lead to the same stability conclusions. It's when terms are dropped to simplify their analysis that they are no longer equivalent, one to another. Prior work by our group and others computed the zero dynamics starting from the essential dynamics (24), resulting in the equations given in (27). In this form, the zero dynamics may as well be a black box because the terms in the reduced-order model seem to have a complicated relationship to the overall physical model of the robot and the virtual constraints. This was not an issue in [27], where feedback control designs were performed by parameterizing the virtual constraints via Beziér polynomials, and then using parameter optimization to minimize the integral-norm squared of the motor torques normalized by distance travelled, subject to constraints on ground reaction forces, joint limits, torque limits, foot clearance, and a desired walking speed.

We next look at the various coordinate representations in (28), (29), and (30).

Case 3: ($\xi_1 = \theta_c, \xi_2 = L$). In (30), the pendulum length r_c depends on the body coordinates q_b while L_c depends on q_b and \dot{q}_b . If we assume that one of the virtual constraints regulates r_c to a known function of (θ_c, L, τ) , which in many cases may depend only on τ or be a constant, then the remaining term for determining the zero dynamics is L_c . If one argues that the effect of L_c is negligible, then the zero dynamics is

$$\begin{aligned} \dot{\theta}_c &= \frac{L}{mr_c^2(\theta_c, L, \tau)} \\ \dot{L} &= mgr_c(\theta_c, L, \tau) \sin(\theta_c) \\ \dot{\tau} &= 1. \end{aligned} \quad (49)$$

If L_c is not negligible, then we've shown a simple way to estimate it online. Otherwise, one needs to compute $L_c(\theta_c, L, \tau)$ using the model (1) and the virtual constraints, through (19) or (26).

Case 2: ($\xi_1 = x_c, \xi_2 = L$). In (29), the height of the center of mass depends on q (and not just q_b) and \dot{z}_c depends on q and \dot{q} . As before L_c depends on q_b and \dot{q}_b . If we assume that one of the virtual constraints regulates z_c to a known function of (θ_c, L, τ) , which in many cases may depend only on τ or be a constant, then the remaining term for determining the zero dynamics is L_c . If one argues that the effect of L_c is negligible, then the zero dynamics is

$$\begin{aligned} \dot{x}_c &= \frac{L}{mz_c(x_c, L, \tau)} + \frac{\dot{z}_c(x_c, L, \tau)}{z_c(x_c, L, \tau)} x_c \\ \dot{L} &= mgx_c \\ \dot{\tau} &= 1. \end{aligned} \quad (50)$$

If L_c is not negligible, then the remarks made above for Case 3 apply.

Case 1: ($\xi_1 = x_c, \xi_2 = v_c^x$). We saved this case for last because v_c^x having relative degree one with respect to the motor torques makes it more technical to derive the zero dynamics directly from the essential dynamics (28) when the virtual constraint to regulate z is allowed to depend on x_c and L . On the other hand, if the virtual constraint to regulate z_c is restricted to a known function of only τ , for example, a constant, then deriving the zero dynamics is straightforward. If one further assumes that the effect of \dot{L}_c is negligible, then the zero dynamics is

$$\begin{aligned} \dot{x}_c &= v_c^x \\ \dot{v}_c^x &= \frac{g + \ddot{z}_c(\tau)}{z_c(\tau)} x_c \\ \dot{\tau} &= 1. \end{aligned} \quad (51)$$

If \dot{L}_c is not negligible, it should be possible to adapt our proposed method for estimating L_c to this case. Otherwise, the work in [78] on Partial Hybrid Zero Dynamics shows how to carefully partition the virtual constraints into a portion that is relative degree one and a portion that is relative degree two and still complete the control design with rigorous theorems on closed-loop stability.

Remark: Suppose that z_c (or r_c) is regulated to a constant value via the virtual constraints and the effects of L_c are negligible. Then (42) and (43) become (or (47) becomes) the zero dynamics.

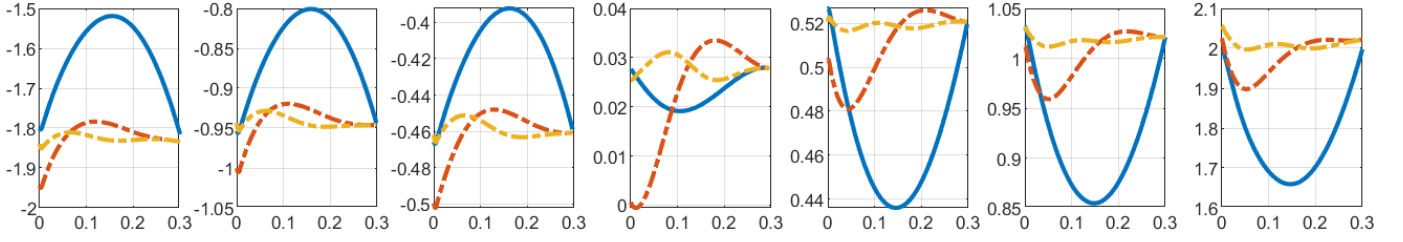


Fig. 9: Prediction of angular momentum about the contact point at the end of a step, when Rabbit is walking at different speed. The **blue** line is the actual evolution of L in the simulation. The **red** line is the predicted value of L at step end when assuming $L_c = 0$. The **yellow** line utilizes a predicted trajectory for L_c . The x -axis is time in seconds. The **yellow** prediction is not perfectly flat because of fitting error in $L_c(t)$ and slight variation of CoM height in the simulation.

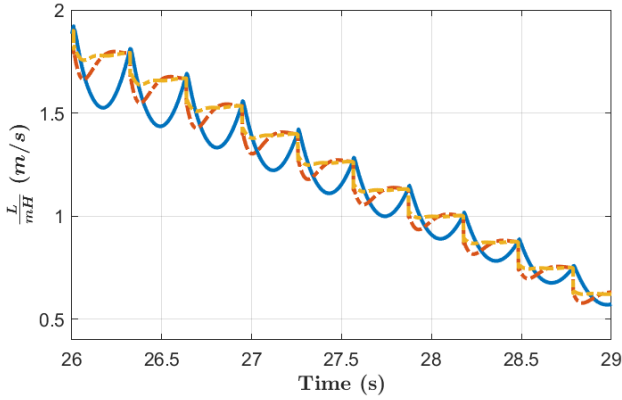


Fig. 10: Though we make the bold assumption that the evolution of $L_c(t)$ over a step depends only on $L(0)$, the value of L at the beginning of a step, the improvement in the one-step-ahead prediction of L persists as walking speed decreases over three seconds from approximately 1.6 m/s to 0.6 m/s. The **blue** line is $L/(mH)$, the **red** line is the estimated value of $L/(mH)$ at the end of the current step when L_c is ignored, and the **yellow** line is the estimated value of $L/(mH)$ at the end of the current step when L_c is estimated each step from $L(0)$. The x -axis is time in seconds.

F. Energy Interpretation of Stabilization Mechanisms

If the virtual constraints have the form $y = q_b - h_d(q_0)$, then the zero dynamics (27) becomes time-invariant and simplifies to

$$\begin{aligned}\dot{\xi}_1 &= \frac{\xi_2}{\kappa_2(\xi_1)} \\ \dot{\xi}_2 &= \kappa_3(\xi_1),\end{aligned}\quad (52)$$

with $\kappa_2(\xi_1) > 0$. In [9, Chap 5.4], it is shown that (52) is Hamiltonian, with

$$\begin{aligned}\mathcal{K}_{\text{zero}} &= \frac{1}{2} \xi_2^2 \\ \mathcal{V}_{\text{zero}} &= - \int_{\xi_1^*}^{\xi_1} \kappa_2(\xi) \kappa_3(\xi) d\xi,\end{aligned}\quad (53)$$

where ξ_1^* is a constant, and that the reset map for the hybrid zero dynamics is

$$\Delta_{\text{zero}}(\xi_1^-, \xi_2^-) = \begin{bmatrix} \xi_1^* \\ \delta_{\text{zero}} \xi_2^- \end{bmatrix}, \quad (54)$$

where δ_{zero} is also a constant.

From (53), it follows that the pseudo total energy

$$\frac{1}{2} \xi_2^2 - \frac{1}{2} mg(x_c)^2$$

is constant along trajectories of (52), and that the impact map resets the potential energy term to the same initial value at each step, while the kinetic energy term changes step to step by

$$\mathcal{K}_{\text{zero}}(\xi_2^+) = (\delta_{\text{zero}})^2 \mathcal{K}_{\text{zero}}(\xi_2^-). \quad (55)$$

Reference [9, Chap 5.4] goes on to show that if the hybrid zero dynamics has a fixed point, then it is locally exponentially stable if, and only if, $0 < (\delta_{\text{zero}})^2 < 1$.

It follows that the stability mechanism for the hybrid zero dynamics (52) and (57) is through the modification of the kinetic energy term at step transitions. We show next that for the ALIP model (43), the stability mechanism is through the modification of a potential energy term at step transitions.

Straightforward calculations show that (43) is Hamiltonian with

$$\begin{aligned}\mathcal{K}_{\text{zero}} &= \frac{1}{2} \frac{L^2}{mH} \\ \mathcal{V}_{\text{zero}} &= -\frac{1}{2} mg(x_c)^2,\end{aligned}\quad (56)$$

which is similar to orbital energy introduced in [79]. Under the assumptions that $z_c \equiv H$, a constant, and the ground is flat, the reset map is

$$\begin{bmatrix} x_c^+ \\ L^+ \end{bmatrix} = \Delta_{\text{zero}}(x_c^-, L^-) = \begin{bmatrix} p_{\text{sw} \rightarrow \text{CoM}}^{x-} \\ L^- \end{bmatrix}, \quad (57)$$

where $p_{\text{sw} \rightarrow \text{CoM}}$ is the vector emanating from the end of the swing leg to the center of mass and $p_{\text{sw} \rightarrow \text{CoM}}^x$ is its x -component. From (56), it follows that the pseudo total energy

$$\frac{1}{2} \frac{L^2}{mH} - \frac{1}{2} mg(x_c)^2$$

is constant along trajectories of (43). From (57), the impact map leaves the kinetic energy term constant while the potential energy term changes step to step by

$$\mathcal{V}_{\text{zero}}(x_c^+) = -\frac{1}{2} mg(p_{\text{sw} \rightarrow \text{CoM}}^{x-})^2. \quad (58)$$

It follows that the stability mechanism is through the modification of the potential energy term at step transitions.

Remark: Appendix B shows how the conservation of pseudo total energy during a step and its change at transitions through the potential energy term motivate a one-step look-ahead controller for the placement of the swing foot.

V. HIGH-LEVEL CONTROL STRATEGY IN TERMS OF ANGULAR MOMENTUM

In this section, we explain our method for deciding where to end one step by initiating contact between the ground and the swing foot, thereby beginning the next step. In robot locomotion, this is typically called⁶ “foot placement control”. Because of the advantages of angular momentum versus linear velocity that we listed in Sect. III-D and IV, we will use angular momentum about the contact point as the primary control variable. To make things as clear as possible, we’ll base the controller on the ALIP model (43) which is a linear and time-invariant approximation of the zero dynamics. In Appendix C, we provide a similar result for nonlinear and time-varying zero dynamics.

A. Selection of virtual constraints

We make the following additional assumptions on the virtual constraints in (13), beyond those already made in (14) and (15):

- (a) the height of the center of mass is regulated to a constant, that is $z_c \equiv H > 0$;
- (b) the step duration is regulated to a constant T ; and
- (c) the horizontal position of the swing leg can be regulated to a desired value, $p_{\text{sw} \rightarrow \text{CoM}}^{\text{des}}$, at the end of the step.

We’ll explain how to accomplish the last item in Sect. VI.

B. Notation

We need to distinguish among the following time instances when specifying the control variables. The superscripts $+$ and $-$ on T_k are necessary because of the (potential) jump in a trajectory’s values from the impact map; see [80]. As shown in Fig. 11, $x(T_k^-)$ is the limit from the left of the model’s solution at the time of impact, in other words it’s value “just before” impact, while $x(T_k^+)$ is the limit from the right of the model’s solution at the time of impact, in other words it’s value “just after” impact.

- T is the step time.
- T_k is the time of the k th impact and thus equals kT .
- T_k^- is the end time of step k , so that
- T_k^+ is the beginning time of step $k+1$ and T_{k+1}^- is the end time of step $k+1$.
- $(T_k^- - t) = (T - \tau(t))$ is the time until the end of step k .

We remind the reader that

- $p_{\text{st} \rightarrow \text{CoM}}$, $p_{\text{sw} \rightarrow \text{CoM}}$ are the vectors emanating from stance/swing foot to the robot’s center of mass. The stance foot defines the current contact point, while the

⁶What else is there to control, one might ask? The overall posture of the robot is very important too.

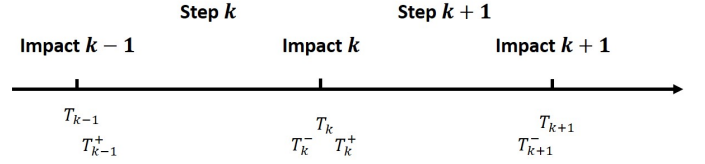


Fig. 11: For a given time, T_k , the notation T_k^- means that we are evaluating a function as a limit from the left of T_k , while T_k^+ means we are taking a limit from the right. This is compatible with how trajectories are defined for the hybrid model (6).

swing foot is defining the point of contact for the next impact and is therefore a control variable.

- Also, because Cassie is 3D, we need to distinguish between L^y and L^x , the y and x components of the angular momentum (sagittal and frontal planes, respectively).

C. Foot placement in longitudinal direction

The control objective will be to place the swing foot at the end of the current step so as to achieve an angular momentum objective at the end of the ensuing step. The need to regulate the angular momentum one-step ahead of the current step, instead of during the current step, is because in (43) L is passive, in other words, it is not affected by the control actions of the current step. The only way to act on its states is through the transition events.

The closed-form solution of (43) at time T and initial time t_0 is

$$\begin{bmatrix} x_c(T) \\ L^y(T) \end{bmatrix} = A(T - t_0) \begin{bmatrix} x_c(t_0) \\ L^y(t_0) \end{bmatrix}, \quad (59)$$

where

$$A(t) = \begin{bmatrix} \cosh(\ell(t)) & -1/mH\ell \sinh(\ell(t)) \\ -mH\ell \sinh(\ell(t)) & \cosh(\ell(t)) \end{bmatrix}$$

and $\ell = \sqrt{\frac{g}{H}}$.

In the following, we breakdown the evolution of L^y from t to T_{k+1}^- , for three key time intervals or instances with the aim of forming a one-step-ahead estimate of angular momentum about the contact point.

1) *From t to T_k^- :* From the second row of (59), an *estimate* for the angular momentum about the contact point at the end of current step, $\hat{L}^y(T_k^-, t)$, can be continuously updated by

$$\begin{aligned} \hat{L}^y(T_k^-, t) = & mH\ell \sinh(\ell(T_k^- - t))x_c(t) \\ & + \cosh(\ell(T_k^- - t))L^y(t). \end{aligned} \quad (60)$$

Forming the running estimate in (60), versus a fixed estimate based on the values of x_c and L^y at the beginning of the step, allows disturbances to be taken into account.

2) *From T_k^- to T_k^+ :* If the CoM height is constant and the ground is flat, the angular momentum about the next contact point will be equal to the angular momentum about the current stance leg, yielding

$$\hat{L}^y(T_k^+, t) = \hat{L}^y(T_k^-, t); \quad (61)$$

see (35). What’s more, the swing foot before impact will become the stance foot after impact,

$$x_c(T_k^+) := p_{\text{st} \rightarrow \text{CoM}}^x(T_k^+) = p_{\text{sw} \rightarrow \text{CoM}}^x(T_k^-). \quad (62)$$

3) *From T_k^+ to T_{k+1}^-* : Similar to (60), the angular momentum at the end of the next step is estimated by

$$\hat{L}^y(T_{k+1}^-, t) = mH\ell \sinh(\ell T)x_c(T_k^+) + \cosh(\ell T)\hat{L}^y(T_k^+, t). \quad (63)$$

Solving (60)-(63) so that

$$\hat{L}^y(T_{k+1}^-, t) = L^{y \text{ des}}(T_{k+1}^-),$$

a desired value of angular momentum, yields a formula for the desired swing foot position at the end of the *current* step, given the value of desired angular momentum at the end of the *next* step,

$$p_{\text{sw} \rightarrow \text{CoM}}^x(T_k^-, t) := \frac{L^{y \text{ des}}(T_{k+1}^-) - \cosh(\ell T)\hat{L}^y(T_k^-, t)}{mH\ell \sinh(\ell T)}. \quad (64)$$

Remark: An identical control law can be derived for (47) if $p_{\text{st} \rightarrow \text{CoM}}^x$ and $p_{\text{sw} \rightarrow \text{CoM}}^x$ are replaced with “ $r_{\text{st} \rightarrow \text{CoM}}$ ” and “ $r_{\text{sw} \rightarrow \text{CoM}}$ ” in the above derivation.

D. Lateral Control and Turning

From (9), the time evolution of the angular momentum about the contact point is decoupled about the x - and y -axes. Therefore, once a desired angular momentum at the end of next step is given, Lateral Control is essentially identical to Longitudinal Control and (64) can be applied equally well in the lateral direction. **The question becomes how to decide on $L^{x \text{ des}}(T_{k+1}^-)$** , since it cannot be simply set to zero for walking with a non-zero stance width.

For walking in place or walking with zero average lateral velocity, it is sufficient to obtain $L^{x \text{ des}}$ from a periodically oscillating LIP model,

$$L^{x \text{ des}}(T_{k+1}^-) = \pm \frac{1}{2}mHW \frac{\ell \sinh(\ell T)}{1 + \cosh(\ell T)}, \quad (65)$$

where W is the desired step width. The sign is positive if next stance is left stance and negative if next stance is right stance. Lateral walking can be achieved by adding an offset to $L^{x \text{ des}}$.

To enable turning, we assume a target direction is commanded and associate a frame to it by aligning the x -axis with the target direction while keeping the z -axis vertical. To achieve turning, we then define the desired angular momentum $L^{y \text{ des}}$ and $L^{x \text{ des}}$ in the new frame and use the hip yaw-motors to align the robot in that direction.

VI. IMPLEMENTING THE LIP-BASED ANGULAR MOMENTUM CONTROLLER ON A REAL ROBOT

In this section we introduce the control variables for Cassie Blue and generate their reference trajectories. As in [33], we leave the stance toe passive. Consequently, there are nine (9) control variables, listed below from the top of the robot to the end of the swing leg,

$$h_0 = \begin{bmatrix} \text{torso pitch} \\ \text{torso roll} \\ \text{stance hip yaw} \\ \text{swing hip yaw} \\ p_{\text{st} \rightarrow \text{CoM}}^z \\ p_{\text{sw} \rightarrow \text{CoM}}^x \\ p_{\text{sw} \rightarrow \text{CoM}}^y \\ p_{\text{sw} \rightarrow \text{CoM}}^z \\ \text{swing toe absolute pitch} \end{bmatrix}. \quad (66)$$

For later use, we denote the value of h_0 at the beginning of the current step by $h_0(T_{k-1}^+)$. When referring to individual components, we'll use $h_{03}(T_{k-1}^+)$, for example.

We first discuss variables that are constant. The reference values for torso pitch, torso roll, and swing toe absolute pitch are constant and zero, while the reference for $p_{\text{st} \rightarrow \text{CoM}}^z$, which sets the height of the CoM with respect to the ground, is constant and equal to H .

We next introduce a phase variable

$$s := \frac{t - T_{k-1}^+}{T} \quad (67)$$

that will be used to define quantities that vary throughout the step to create “leg pumping” and “leg swinging”. The reference trajectories of $p_{\text{sw} \rightarrow \text{CoM}}^x$ and $p_{\text{sw} \rightarrow \text{CoM}}^y$ are defined such that:

- at the beginning of a step, their reference value is their actual position;
- the reference value at the end of the step implements the foot placement strategy in (64); and
- in between a half-period cosine curve is used to connect them, which is similar to the trajectory of an ordinary (non-inverted) pendulum.

The reference trajectory of $p_{\text{sw} \rightarrow \text{CoM}}^z$ assumes the ground is flat and the control is perfect:

- at mid stance, the height of the foot above the ground is given by z_{CL} , for the desired vertical clearance.

The reference trajectories for the stance hip and swing hip yaw angles are simple straight lines connecting their initial actual position and their desired final positions. For walking in a straight line, the desired final position is zero. To include turning, the final value has to be adjusted. Suppose that a turn angle of ΔD_k^{des} radians is desired. One half of this value is given to each yaw joint:

- $+\frac{1}{2}\Delta D_k^{\text{des}} \rightarrow$ swing hip yaw; and
- $-\frac{1}{2}\Delta D_k^{\text{des}} \rightarrow$ stance hip yaw

The signs may vary with the convention used on other robots.

The final result for Cassie Blue is

$$h_d(s) := \begin{bmatrix} 0 \\ 0 \\ (1-s)h_{03}(T_{k-1}^+) + s(-\frac{1}{2}(\Delta D_k)) \\ (1-s)h_{04}(T_{k-1}^+) + s(\frac{1}{2}(\Delta D_k)) \\ H \\ \frac{1}{2}[(1 + \cos(\pi s))h_{06}(T_{k-1}^+) + (1 - \cos(\pi s))p_{\text{sw} \rightarrow \text{CoM}}^x(T_k^-)] \\ \frac{1}{2}[(1 + \cos(\pi s))h_{07}(T_{k-1}^+) + (1 - \cos(\pi s))p_{\text{sw} \rightarrow \text{CoM}}^y(T_k^-)] \\ 4z_{cl}(s - 0.5)^2 + (H - z_{CL}); \\ 0 \end{bmatrix}. \quad (68)$$

When implemented with an Input-Output Linearizing Controller⁷ so that h_0 tracks h_d , the above control policy allows Cassie to move in 3D in simulation.

VII. PRACTICAL IMPLEMENTATION ON CASSIE

This section resolves several issues that prevent the basic controller from being implemented on Cassie Blue.

⁷The required kinematic and dynamics functions are generated with FROST [81].

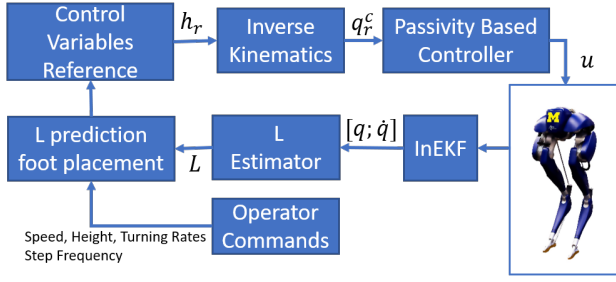


Fig. 12: Block diagram of the implemented controller.

A. IMU and EKF

In a real robot, an IMU and an EKF are needed to estimate the linear position and rotation matrix at a fixed point on the robot, along with their derivatives. Cassie uses a VectorNav IMU. We used the Contact-aided Invariant EKF developed in [82], [83] to estimate the torso velocity. With these signals in hand, we could estimate angular momentum about the contact point.

B. Filter for Angular Momentum

Angular Momentum about the contact toe could be estimated directly from the sensors on the robot, but it is noisy. We designed a Kalman Filter to improve the estimation. The models we used are

$$\text{Prediction: } L^y(k+1) = L^y(k) + m g p_{st}(k) \Delta T + \delta(k)$$

$$\text{Correction: } L^y(k) = L^y_{\text{obs}}(k) + \epsilon(k) \quad (69)$$

C. Inverse Kinematics

Input-Output Linearization does not work well in experiments [33], [84], [85]. To use a passivity-based controller for tracking that is inspired by [61], we need to convert the reference trajectories for the variables in (66) to reference trajectories for Cassie's actuated joints,

$$q^{\text{act}} = \begin{bmatrix} \text{torso pitch} \\ \text{torso roll} \\ \text{stance hip yaw} \\ \text{swing hip yaw} \\ \text{stance knee pitch} \\ \text{swing hip roll} \\ \text{swing hip pitch} \\ \text{swing knee pitch} \\ \text{swing toe pitch} \end{bmatrix}. \quad (70)$$

Iterative inverse kinematics is used to convert the controlled variables in (66) to the actuated joints.

D. Passivity-based Controller

We adapt the passivity-based controller developed in [61] to achieve joint-level tracking. This method takes the full-order model of robot into consideration and, on a perfect model, will drive the virtual constraints asymptotically to zero. The derivation is given in the Appendix.

E. Springs

On the swing leg, the spring deflection is small and thus we are able to assume the leg to be rigid. On the stance leg, the spring deflection is non-negligible and hence requires compensation. While there are encoders on both sides of the spring to measure its deflection, direct use of this leads to oscillations. The deflection of the spring is instead estimated through a simplified model.

F. COM Velocity in the Vertical Direction

When Cassie is walking speed exceeds one meter per second, the assumption that $v_{\text{CoM}}^z \approx 0$ breaks down and (61) is no longer valid. Hence, we use

$$L^y(T_k^+) = L^y(T_k^-) + m v_c^z(T_k^-) (p_{\text{sw} \rightarrow \text{CoM}}^x(T_k^-) - p_{\text{st} \rightarrow \text{CoM}}^x(T_k^-)). \quad (71)$$

From this, the foot placement is updated to

$$p_{\text{sw} \rightarrow \text{CoM}}^x(T_k^-) = \frac{L^y \text{des}(T_{k+1}^-) - (L^y(T_k^-) + m v_{\text{CoM}}^z(T_k^-) p_{\text{st} \rightarrow \text{CoM}}^x(T_k^-)) \cosh(\ell T)}{m(H\ell \sinh(\ell T) - v_{\text{CoM}}^z \cosh(\ell T))}. \quad (72)$$

VIII. EXPERIMENTAL RESULTS

The controller was implemented on Cassie Blue. The closed-loop system consisting of robot and controller was evaluated in a number of situations that are itemized below.

- **Walking in a straight line on flat ground.** Cassie could walk in place and walk stably for speeds ranging from zero to 2.1 m/s.
- **Diagonal Walking.** Cassie is able to walk simultaneously forward and sideways on grass, at roughly 1 m/s in each direction.
- **Sharp turn.** While walking at roughly 1 m/s, Cassie Blue effected a 90° turn in six steps, without slowing down.
- **Rejecting the classical kick to the base of the hips.** Cassie was able to remain upright under “moderate” kicks in the longitudinal direction. The disturbance rejection in the lateral direction is not as robust as the longitudinal, which is mainly caused by Cassie’s physical design: small hip roll motor position limits.
- **Finally we address walking on rough ground.** Cassie Blue was tested on the iconic Wave Field of the University of Michigan North Campus. The foot clearance was increased from 10 cm to 20 cm to handle the highly undulating terrain. Cassie is able to walk through the “valley” between the large humps with ease at a walking pace of roughly 0.75 m/s, without falling in all tests. The row of ridges running east to west in the Wave Field are roughly 60 cm high, with a sinusoidal structure. We estimate the maximum slope to be 40 degrees. Cassie is able to cross several of the large humps in a row, but also fell multiple times. On a more gentle, straight grassy slope of roughly 22 degrees near the laboratory, Cassie can walk up it with no difficulty with 20cm foot clearance.

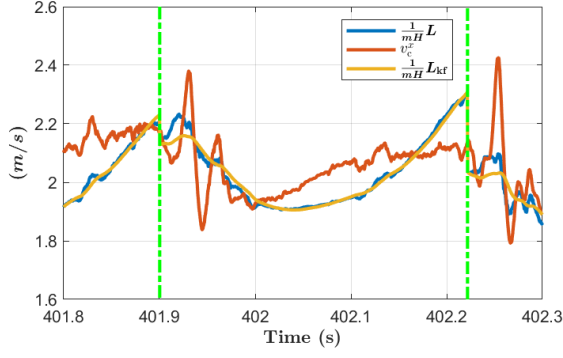


Fig. 13: Experimental data from Cassie walking forward at about 2m/s. v_c^x oscillates because of sensor noise and its relative degree one nature, which means it is heavily affected by motor torques and spring oscillation. L is mostly smooth because it is relative degree three, except near impact when the robot is in double support phase and L has relative degree one. Applying the Kalman filter described in Sect. VII-B, results L_{kf} in which small oscillations caused by sensor noise are removed. The sudden jump in L at impact is caused by nonzero v_c^z .

IX. CONCLUSIONS

We established connections between various approximate pendulum models that are commonly used for heuristic controller design and those that are more common in the feedback control literature where formal stability guarantees are the norm. The paper sought to bring these two communities together, clarifying their commonalities and differences. In the process of doing so, we argued that models based on angular momentum about the contact point provide more accurate representations of robot state than models based on linear velocity. Specifically, we showed that an approximate (pendulum or zero dynamics) model parameterized by angular momentum provides better predictions for foot placement on a physical robot (e.g., legs with mass) than does a related approximate model parameterized in terms of linear velocity. Because of the weakly actuated nature of angular momentum about the contact point, it needs to be regulated step-to-step and not within a step. We implemented a one-step-ahead angular-momentum-based controller on Cassie, a 3D robot, and demonstrated high agility and robustness in experiments. Using our new controller, Cassie was able to accomplish a wide range of tasks with nothing more than common sense task-based tuning: a higher step frequency to walk at 2.1 m/s and extra foot clearance to walk over slopes exceeding 22 degrees. Moreover, in the current implementation, there is no optimization of trajectories used in the implementation on Cassie. The robot's performance is currently limited by the hand-designed trajectories leading to joint-limit violations and foot slippage. These limitations will be mitigated by incorporating optimization.



Fig. 14: Images from several closed-loop experiments conducted with Cassie Blue and the controller developed in this paper. A short video compilation of these experiments is available in [86]. Longer versions can be found in [87].

APPENDIX

A. Passivity-based Input-Output Stabilization

The material presented here adapts the original work in [61] to a floating-base model

$$D(q)\ddot{q} + H(q, \dot{q}) = Bu + J_s^\top \tau_s + J_g(q)^\top \tau_g, \quad (73)$$

with u the vector of motor torques, τ_s the spring torques, and τ_g is the contact wrench. During the single support phase, the blade-shape foot on Cassie provides five holonomic constraints, leaving only foot roll free. To simplify the problem, we also assume the springs are rigid, adding two constraint on each leg. These constraints leave the original 20-degree-of-freedom floating base model with 11 degrees of freedom.

The constraints mentioned above can be written as

$$\begin{cases} J_s \ddot{q} = 0 \\ J_g(q) \ddot{q} + \dot{J}_g(q) \dot{q} = 0. \end{cases} \quad (74)$$

Combining (73) and (74) yields the full model for Cassie in single support,

$$\underbrace{\begin{bmatrix} D & -J_s^\top & -J_g^\top \\ J_s & 0 & 0 \\ J_g & 0 & 0 \end{bmatrix}}_{\bar{D}} \underbrace{\begin{bmatrix} \ddot{q} \\ \tau_s \\ \tau_g \end{bmatrix}}_f + \underbrace{\begin{bmatrix} H \\ 0 \\ \dot{J}_g \dot{q} \end{bmatrix}}_{\bar{H}} = \underbrace{\begin{bmatrix} B \\ 0 \\ 0 \end{bmatrix}}_{\bar{B}} u \quad (75)$$

For simplicity we assume that the components of q have already been ordered such that $q = [q_c, q_u]^T$, where q_c are the coordinates chosen to be controlled and q_u are the free coordinates. Define $\lambda = [q_u, \tau_s, \tau_g]^T$ and partition (75) as

$$\begin{cases} \tilde{D}_{11}\ddot{q}_c + \tilde{D}_{12}\lambda + \tilde{H}_1 = \tilde{B}_1 u \\ \tilde{D}_{21}\ddot{q}_c + \tilde{D}_{22}\lambda + \tilde{H}_2 = \tilde{B}_2 u \end{cases} \quad (76)$$

The vector λ can be eliminated from these equations, resulting in

$$\bar{D}\ddot{q}_c + \bar{H} = \bar{B}u, \quad (77)$$

where

$$\begin{aligned} \bar{D} &= \tilde{D}_{11} - \tilde{D}_{12}\tilde{D}_{22}^{-1}\tilde{D}_{21} \\ \bar{H} &= \tilde{H}_1 - \tilde{D}_{12}\tilde{D}_{22}^{-1}\tilde{H}_2 \\ \bar{B} &= \tilde{B}_1 - \tilde{D}_{12}\tilde{D}_{22}^{-1}\tilde{B}_2. \end{aligned}$$

We note that \tilde{D}_{22} being invertible and \bar{D} being positive definite both follow from \tilde{D} being positive definite. Later, we need \bar{B} to be invertible; *this is an assumption* similar to that in (14). Equation (77) is what we will focus on from here on.

For the Passivity-based Controller, the error dynamic for $y := q_c - q_r$ and is designed to be [88]

$$\bar{D}\ddot{y} + (\bar{C} + k_d)\dot{y} + k_p y = 0, \quad (78)$$

where \bar{C} is the Coriolis/centrifugal matrix in \bar{H} and it is chosen such that $\dot{\bar{D}} = \bar{C} + \bar{C}^\top$. From (77) and (78), we have

$$u = \bar{B}^{-1}(\bar{D}\ddot{q}_r + \bar{H}) - \bar{B}^{-1}(k_p y + (\bar{C} + k_d)\dot{y}). \quad (79)$$

Compared with a standard Input-Output Linearization controller, whose error dynamics and command torque are

$$\ddot{y} + k_d \dot{y} + k_p y = 0, \quad \text{and} \quad (80)$$

$$u = \bar{B}^{-1}(\bar{D}\ddot{q}_r + \bar{H}) - \bar{B}^{-1}\bar{D}(k_p y + k_d \dot{y}), \quad (81)$$

the passivity-based controller induces less cancellation of the robot's dynamics, and if k_p and k_d are chosen to be diagonal matrices, the tracking errors are approximately decoupled because, for Cassie, \bar{B}^{-1} is close to diagonal. This controller provides improved tracking performance over the straight-up PD implementation in [33].

B. A One-step Ahead Deadbeat Controller Based on Total Energy for the ALIP

We rewrite (59) as

$$\begin{bmatrix} x_c(T) \\ L(T) \end{bmatrix} = A(T) \begin{bmatrix} x_c(0) \\ L(0) \end{bmatrix}$$

and seek “fixed points”, that is, conditions for periodicity when the impact map is included. With $\dot{z}_c = 0$, we have $L(T) = L(0)$, and a straightforward calculation with (59) shows that

$$L(T) = L(0) \implies x_c(T) = -x_c(0)$$

and hence periodic gaits are symmetric. Another straightforward calculation shows that if

$$\begin{bmatrix} x_c^* \\ L^* \end{bmatrix} = A(T) \begin{bmatrix} -x_c^* \\ L^* \end{bmatrix},$$

then

$$\frac{x_c^*}{L^*} = -\frac{1}{mH\ell} \frac{\sinh(\ell T)}{1 + \cosh(\ell T)} = -\frac{1}{mH\ell} \frac{\cosh(\ell T) - 1}{\sinh(\ell T)}$$

and one easily shows that

$$\frac{\sinh(t)}{1 + \cosh(t)} = \frac{\cosh(t) - 1}{\sinh(t)} = \frac{1 - e^{-t}}{1 + e^{-t}}.$$

For a symmetric gait with constant step duration T the average speed is $v_c^{x,\text{avg}} = 2 \frac{x_c(T)}{T}$. It follows that for a prescribed average walking speed, $v_c^{x,\text{avg}}$, the fixed points satisfy

$$\begin{aligned} x_c^* &= \frac{T}{2} v_c^{x,\text{avg}} \\ L^* &= -mH\ell \left(\frac{1 + e^{-\ell T}}{1 - e^{-\ell T}} \right) \frac{T}{2} v_c^{x,\text{avg}}. \end{aligned}$$

After a bit of algebra, the (pseudo) energy associated with a fixed point can then be written as

$$\begin{aligned} E^*(v_c^{x,\text{avg}}) &= \frac{1}{2} mg \left(\frac{T}{2} v_c^{x,\text{avg}} \right)^2 \left[\left(\frac{1 + e^{-\ell T}}{1 - e^{-\ell T}} \right)^2 - 1 \right] \\ &= 2mg \left(\frac{T}{2} v_c^{x,\text{avg}} \right)^2 \frac{e^{-\ell T}}{(1 - e^{-\ell T})^2}. \end{aligned}$$

We take the control objective to be $E(T_k^+) = E^*$, which of course, would need to be achieved subject to work space limits. If we assume that

$$L(T_k^+) = \hat{L}(T_k^-),$$

our control law results from solving

$$-\frac{1}{2} mg (p_{\text{sw} \rightarrow \text{CoM}}^x(T_k^-))^2 + \frac{1}{2} \frac{1}{mH} \left(\hat{L}(T_k^-) \right)^2 = E^*(v_c^{x,\text{des}})$$

for the desired swing foot position, to achieve a desired energy for step $k+1$. This is a one-step-ahead control law where we only need to run the angular momentum estimator for the end of the current step.

C. One Step-ahead Foot Placement with Nonlinear Time-varying Zero Dynamics

Section V-C presented in (64) a closed-form solution for where to place the swing foot at the end of a given step in order to achieve a desired angular momentum at the end of the ensuing step. This formula exploited the availability of a closed-form solution for a linear time-invariant approximation of the zero dynamics. Here we'll show how to place the swing foot at the end of a given step in order to achieve a *desired*

angular momentum at the end of the next step for the more general case of a possibly time-varying, nonlinear dynamics with states $\xi_1 = x_c, \xi_2 = L, \xi_3 = \tau$, along with remarks for a practical real-time implementation of the resulting formulas. We assume that virtual constraints are designed such that

- (a) the step duration is regulated to a constant T ; and
- (b) the horizontal position of the swing leg can be regulated to a desired value, $p_{sw \rightarrow CoM}^{x, des}$, at the end of a step.

We also assume that the impact map (56) has been updated as in (71) so that the center of mass height may vary and that it includes $\tau^+ = 0$.

For notational compactness, let $p_{sw} := p_{sw \rightarrow CoM}^{x, des}$, the desired horizontal position of the swing foot, which we treat as a control parameter. For $0 \leq \tau < T$, let

$$\varphi_{\tau}^{p_{sw}^{des}}(\xi_{1,0}, \xi_{2,0}, \tau_0) \quad (82)$$

denote the solution of the zero dynamics (22), or any of its approximations treated in Sect. IV-E, with initial condition $(\xi_{1,0}, \xi_{2,0}, \tau_0)$ and value for p_{sw}^{des} . Also, let π_2 pick off the second component of a vector. Then, for given values of p_{sw}^{curr} for the current step and p_{sw}^{nxt} for the next step, we can predict the value of the angular momentum at the end of the next step by

$$\begin{aligned} \hat{L}(T_{k+1}^-, \tau, p_{sw}^{curr}, p_{sw}^{nxt}) &= \pi_2 \circ \varphi_T^{p_{sw}^{nxt}} \circ \Delta_{zero} \circ \\ &\quad \circ \varphi_T^{p_{sw}^{curr}}(\xi_1(\tau), \xi_2(\tau), \tau). \end{aligned} \quad (83)$$

With the step time fixed, the planned position for the swing foot at the next step has very little effect on $\hat{L}(T_{k+1}^-)$, so we assign a nominal value to it, say

$$p_{sw}^{nxt} := \frac{T}{2} v_c^{x, avg}.$$

One then solves iteratively offline for $p_{sw}^{curr}(\tau)$, satisfying

$$\hat{L}(T_{k+1}^-, \tau, p_{sw}^{curr}, \frac{T}{2} v_c^{x, avg}) = L^{des}(T_{k+1}^-), \quad (84)$$

for $0 \leq \tau < T$, and store the values for use online. While it is possible to only compute p_{sw}^{curr} for $\tau = 0$, updating it throughout the step allows corrections for disturbances.

ACKNOWLEDGMENT

Toyota Research Institute provided funds to support this work. Funding for J. Grizzle was in part provided by NSF Award No. 1808051.

REFERENCES

- [1] H. Miura and I. Shimoyama. Dynamic walk of a biped. *International Journal of Robotics Research*, 3(2):60–74, 1984.
- [2] Shuuji Kajita, Fumio Kanehiro, Kenji Kaneko, Kazuhito Yokoi, and Hirohisa Hirukawa. The 3d linear inverted pendulum mode: A simple modeling for a biped walking pattern generation. In *Proceedings 2001 IEEE/RSJ International Conference on Intelligent Robots and Systems. Expanding the Societal Role of Robotics in the Next Millennium (Cat. No. 01CH37180)*, volume 1, pages 239–246. IEEE, 2001.
- [3] R. Blickhan. The spring-mass model for running and hopping. *Journal of Biomechanics*, 22(11-12):1217–1227, 1989.
- [4] Jerry Pratt, John Carff, Sergey Drakunov, and Ambarish Goswami. Capture point: A step toward humanoid push recovery. In *2006 6th IEEE-RAS international conference on humanoid robots*, pages 200–207. IEEE, 2006.
- [5] Johannes Engelsberger, Christian Ott, Máximo A Roa, Alin Albu-Schäffer, and Gerhard Hirzinger. Bipedal walking control based on capture point dynamics. In *2011 IEEE/RSJ International Conference on Intelligent Robots and Systems*, pages 4420–4427. IEEE, 2011.
- [6] Ting Wang and Christine Chevallereau. Stability analysis and time-varying walking control for an under-actuated planar biped robot. *Robotics and Autonomous Systems*, 59(6):444 – 456, 2011.
- [7] Xiaobin Xiong and Aaron D Ames. Orbit characterization, stabilization and composition on 3d underactuated bipedal walking via hybrid passive linear inverted pendulum model. In *2019 IEEE/RSJ International Conference on Intelligent Robots and Systems (IROS)*, pages 4644–4651. IEEE, 2019.
- [8] Agility Robotics. Robots. <https://www.agilityrobotics.com/robots#cassie>, 2021.
- [9] E. R. Westervelt, J. W. Grizzle, C. Chevallereau, J. H. Choi, and B. Morris. *Feedback Control of Dynamic Bipedal Robot Locomotion*. Control and Automation. CRC Press, Boca Raton, FL, June 2007.
- [10] T. Yang, E. R. Westervelt, A. Serrani, and J. P. Schmiedeler. A framework for the control of stable aperiodic walking in underactuated planar bipeds. *Autonomous Robots*, 27(3):277–290, 2009.
- [11] Anne E. Martin, David C. Post, and James P. Schmiedeler. Design and experimental implementation of a hybrid zero dynamics-based controller for planar bipeds with curved feet. *The International Journal of Robotics Research*, 33(7):988–1005, 2014.
- [12] H. Zhao, J. Horn, J. Reher, V. Paredes, and A. D. Ames. A hybrid systems and optimization-based control approach to realizing multi-contact locomotion on transfemoral prostheses. In *IEEE Conference on Decision and Control (CDC)*, pages 1607–1612, Dec 2015.
- [13] Jacob Reher, Eric A Cousineau, Ayonga Hereid, Christian M Hubicki, and Aaron D Ames. Realizing dynamic and efficient bipedal locomotion on the humanoid robot durus. In *2016 IEEE International Conference on Robotics and Automation (ICRA)*, pages 1794–1801. IEEE, 2016.
- [14] J. Reher, E. A. Cousineau, A. Hereid, C. M. Hubicki, and A. D. Ames. Realizing dynamic and efficient bipedal locomotion on the humanoid robot DURUS. In *2016 IEEE International Conference on Robotics and Automation (ICRA)*, pages 1794–1801, May 2016.
- [15] Brent Griffin and Jessy Grizzle. Nonholonomic virtual constraints for dynamic walking. In *2015 54th IEEE Conference on Decision and Control (CDC)*, pages 4053–4060. IEEE, 2015.
- [16] Ayush Agrawal, Omar Harib, Ayonga Hereid, Sylvain Finet, Matthieu Masselin, Laurent Praly, Aaron D. Ames, Koushil Sreenath, and Jessy W. Grizzle. First steps towards translating HZD control of bipedal robots to decentralized control of exoskeletons. *IEEE Access*, 5:9919–9934, 2017.
- [17] Thomas Gurriet, Sylvain Finet, Guilhem Boeris, Alexis Duburcq, Ayonga Hereid, Omar Harib, Matthieu Masselin, Jessy Grizzle, and Aaron D Ames. Towards restoring locomotion for paraplegics: Realizing dynamically stable walking on exoskeletons. In *C-ICRA*, pages 2804–2811. IEEE, 2018.
- [18] Xingye Da and Jessy Grizzle. Combining trajectory optimization, supervised machine learning, and model structure for mitigating the curse of dimensionality in the control of bipedal robots. *The International Journal of Robotics Research*, 38(9):1063–1097, 2019.
- [19] A. Isidori. *Nonlinear Control Systems*. Springer-Verlag, Berlin, third edition, 1995.
- [20] C. Byrnes and A. Isidori. Asymptotic stabilization of nonlinear minimum phase systems. *IEEE Transactions on Automatic Control*, 37(6):1122–37, 1991.
- [21] E. R. Westervelt and J. W. Grizzle. Design of asymptotically stable walking for a 5-link planar biped walker via optimization. In *Proc. of the 2002 IEEE International Conference on Robotics and Automation, Washington, D.C.*, pages 3117–22, 2002.
- [22] Ioannis Poulakakis and Jessy W Grizzle. The spring loaded inverted pendulum as the hybrid zero dynamics of an asymmetric hopper. *IEEE Transactions on Automatic Control*, 54(8):1779–1793, 2009.
- [23] Ayonga Hereid, Shishir Kolathaya, Mikhail S. Jones, Johnathan Van Why, Jonathan W. Hurst, and Aaron D. Ames. Dynamic multi-domain bipedal walking with ATRIAS through SLIP based human-inspired control. In *Proceedings of the 17th International Conference on Hybrid Systems: Computation and Control, HSCC '14*, pages 263–272, New York, NY, USA, 2014. ACM.
- [24] Yu-Ming Chen and Michael Posa. Optimal reduced-order modeling of bipedal locomotion. In *2020 IEEE International Conference on Robotics and Automation (ICRA)*, pages 8753–8760. IEEE, 2020.
- [25] Víctor De-León-Gómez, Qiuyue Luo, Anne Kalouguine, J Alfonso Pámanes, Yannick Aoustin, and Christine Chevallereau. An essential model for generating walking motions for humanoid robots. *Robotics and Autonomous Systems*, 112:229–243, 2019.

- [26] Qiuyue Luo, Christine Chevallereau, and Yannick Aoustin. Walking stability of a variable length inverted pendulum controlled with virtual constraints. *International Journal of Humanoid Robotics*, 16(06):1950040, 2019.
- [27] Brent Griffin and Jessy Grizzle. Nonholonomic virtual constraints and gait optimization for robust walking control. *The International Journal of Robotics Research*, page 0278364917708249, 2016.
- [28] Matthew J Powell and Aaron D Ames. Mechanics-based control of underactuated 3d robotic walking: Dynamic gait generation under torque constraints. In *2016 IEEE/RSJ International Conference on Intelligent Robots and Systems (IROS)*, pages 555–560. IEEE, 2016.
- [29] Yukai Gong and Jessy Grizzle. Angular momentum about the contact point for control of bipedal locomotion: Validation in a lip-based controller. *arXiv preprint arXiv:2008.10763 [cs.CV]*, 2020.
- [30] Xingye Da, Omar Harib, Ross Hartley, Brent Griffin, and Jessy W Grizzle. From 2D design of underactuated bipedal gaits to 3D implementation: Walking with speed tracking. *IEEE Access*, 4:3469–3478, 2016.
- [31] Ross Hartley, Xingye Da, and Jessy W. Grizzle. Stabilization of 3D underactuated biped robots: Using posture adjustment and gait libraries to reject velocity disturbances. In *IEEE Conference on Control Technology and Applications (CCTA)*, 2017.
- [32] Omar Harib, Ayonga Hereid, Ayush Agrawal, Thomas Gurriet, Sylvain Finet, Guilhem Boeris, Alexis Duburcq, M. Eva Mungai, Matthieu Masselien, Aaron D. Ames, Koushil Sreenath, and Jessy Grizzle. Feedback control of an exoskeleton for paraplegics: Toward robustly stable hands-free dynamic walking. *arXiv preprint arXiv:1802.08322 [cs.RO]*, 2018.
- [33] Y. Gong, R. Hartley, X. Da, A. Hereid, O. Harib, J. Huang, and J. Grizzle. Feedback control of a cassie bipedal robot: Walking, standing, and riding a segway. In *2019 American Control Conference (ACC)*, pages 4559–4566, 2019.
- [34] Toru Takenaka, Takashi Matsumoto, and Takahide Yoshiike. Real time motion generation and control for biped robot-1 st report: Walking gait pattern generation. In *2009 IEEE/RSJ International Conference on Intelligent Robots and Systems*, pages 1084–1091. IEEE, 2009.
- [35] Jerry Pratt and Gill Pratt. Exploiting natural dynamics in the control of a 3d bipedal walking simulation. In *In Proc. of Int. Conf. on Climbing and Walking Robots (CLAWAR99)*, 1999.
- [36] Siavash Rezazadeh, Christian Hubicki, Mikhail Jones, Andrew Peekema, Johnathan Van Why, Andy Abate, and Jonathan Hurst. Spring-mass walking with atrias in 3D: Robust gait control spanning zero to 4.3 kph on a heavily underactuated bipedal robot. In *ASME 2015 dynamic systems and control conference*, pages V001T04A003–V001T04A003. American Society of Mechanical Engineers, 2015.
- [37] Guillermo A Castillo, Bowen Weng, Wei Zhang, and Ayonga Hereid. Robust feedback motion policy design using reinforcement learning on a 3d digit bipedal robot. *arXiv preprint arXiv:2103.15309*, 2021.
- [38] Zhaoming Xie, Patrick Clary, Jeremy Dao, Pedro Morais, Jonathan Hurst, and Michiel Panne. Learning locomotion skills for cassie: Iterative design and sim-to-real. In *Conference on Robot Learning*, pages 317–329. PMLR, 2020.
- [39] S. Kajita, F. Kanehiro, K. Kaneko, K. Fujiwara, K. Harada, K. Yokoi, and H. Hirukawa. Biped walking pattern generation by using preview control of zero-moment point. In *2003 IEEE International Conference on Robotics and Automation (Cat. No.03CH37422)*, volume 2, pages 1620–1626 vol.2, 2003.
- [40] R. Tedrake, S. Kuindersma, R. Deits, and K. Miura. A closed-form solution for real-time zmp gait generation and feedback stabilization. In *2015 IEEE-RAS 15th International Conference on Humanoid Robots (Humanoids)*, pages 936–940, 2015.
- [41] Min Dai, Xiaobin Xiong, and Aaron Ames. Bipedal walking on constrained footholds: Momentum regulation via vertical com control. *arXiv preprint arXiv:2104.10367*, 2021.
- [42] Hamed Razavi, Anthony M Bloch, Christine Chevallereau, and Jessy W Grizzle. Symmetry in legged locomotion: a new method for designing stable periodic gaits. *Autonomous Robots*, 41(5):1119–1142, 2017.
- [43] Qiuyue Luo, Victor De-León-Gómez, Anne Kalouguine, Christine Chevallereau, and Yannick Aoustin. Self-synchronization and self-stabilization of walking gaits modeled by the three-dimensional lip model. *IEEE Robotics and Automation Letters*, 3(4):3332–3339, 2018.
- [44] Ambarish Goswami, Bernard Espiau, and Ahmed Keramane. Limit cycles in a passive compass gait biped and passivity-mimicking control laws. *Autonomous Robots*, 4(3):273–286, 1997.
- [45] Ian A Hiskens. Stability of hybrid system limit cycles: Application to the compass gait biped robot. In *Proceedings of the 40th IEEE Conference on Decision and Control (Cat. No. 01CH37228)*, volume 1, pages 774–779. IEEE, 2001.
- [46] David Pekarek, Aaron D Ames, and Jerrold E Marsden. Discrete mechanics and optimal control applied to the compass gait biped. In *2007 46th IEEE Conference on Decision and Control*, pages 5376–5382. IEEE, 2007.
- [47] Wafa Znegui, Hassène Gritli, and Safya Belghith. Design of an explicit expression of the poincaré map for the passive dynamic walking of the compass-gait biped model. *Chaos, Solitons & Fractals*, 130:109436, 2020.
- [48] Wei He, Zhijun Li, and CL Philip Chen. A survey of human-centered intelligent robots: issues and challenges. *IEEE/CAA Journal of Automatica Sinica*, 4(4):602–609, 2017.
- [49] J. W. Grizzle, G. Abba, and F. Plestan. Asymptotically stable walking for biped robots: Analysis via systems with impulse effects. *IEEE Transactions on Automatic Control*, 46(1):51–64, January 2001.
- [50] Christine Chevallereau. Time-scaling control for an underactuated biped robot. *IEEE Transactions on Robotics and Automation*, 19(2):362–368, 2003.
- [51] A. D. Ames, E. A. Cousineau, and M. J. Powell. Dynamically stable bipedal robotic walking with NAO via human-inspired hybrid zero dynamics. In *Proceedings of the 15th ACM international conference on Hybrid Systems: Computation and Control*, pages 135–144. ACM, 2012.
- [52] Koushil Sreenath, Hae-Won Park, and J. W. Grizzle. Design and experimental implementation of a compliant hybrid zero dynamics controller with active force control for running on MABEL. In *Int. Conf. on Robotics and Automation (ICRA)*, pages 51–56, Minneapolis, MN USA, May 2012.
- [53] A. E. Martin, D. C. Post, and J. P. Schmiedeler. The effects of foot geometric properties on the gait of planar bipeds walking under HZD-based control. *The International Journal of Robotics Research*, 33(12):1530–1543, 2014.
- [54] Kyle R Embry, Dario J Villarreal, and Robert D Gregg. A unified parameterization of human gait across ambulation modes. In *2016 38th Annual International Conference of the IEEE Engineering in Medicine and Biology Society (EMBC)*, pages 2179–2183. IEEE, 2016.
- [55] Yukai Gong and Jessy Grizzle. One-step ahead prediction of angular momentum about the contact point for control of bipedal locomotion: Validation in a lip-inspired controller. Accepted for IEEE International Conference on Robotics and Automation, 2021.
- [56] C. Chevallereau, G. Abba, Y. Aoustin, F. Plestan, E. R. Westervelt, C. Canudas-de-Wit, and J. W. Grizzle. RABBIT: A testbed for advanced control theory. *IEEE Control Systems Magazine*, 23(5):57–79, October 2003.
- [57] E. Westervelt, J. W. Grizzle, and D.E. Koditschek. Hybrid zero dynamics of planar biped walkers. *IEEE Transactions on Automatic Control*, 48(1):42–56, January 2003.
- [58] Y. Hurmuzlu and T.H. Chang. Rigid body collisions of a special class of planar kinematic chains. *IEEE Transactions on Systems, Man, and Cybernetics*, 22(5):964–971, 1992.
- [59] Y. Hurmuzlu. Dynamics of bipedal gait - part 1: objective functions and the contact event of a planar five-link biped. *Journal of Applied Mechanics*, 60:331–336, June 1993.
- [60] J. W. Grizzle, G. Abba, and F. Plestan. Asymptotically stable walking for biped robots: Analysis via systems with impulse effects. *IEEE Transactions on Automatic Control*, 46:51–64, January 2001.
- [61] Hamid Sadeghian, Christian Ott, Gianluca Garofalo, and Gordon Cheng. Passivity-based control of underactuated biped robots within hybrid zero dynamics approach. In *2017 IEEE International Conference on Robotics and Automation (ICRA)*, pages 4096–4101. IEEE, 2017.
- [62] A. Ames, K. Galloway, J. W. Grizzle, and K. Sreenath. Rapidly exponentially stabilizing control Lyapunov functions and hybrid zero dynamics. *IEEE Transactions on Automatic Control*, 59(4):876–891, 2014.
- [63] A. Isidori. *Nonlinear Control Systems: An Introduction*. Springer-Verlag, Berlin, 2nd edition, 1989.
- [64] K. Sreenath, H.W. Park, I. Poulakakis, and J. W. Grizzle. A compliant hybrid zero dynamics controller for stable, efficient and fast bipedal walking on MABEL. *International Journal of Robotics Research*, 30(9):1170–1193, 2011.
- [65] Yan Gu, Bin Yao, and CS George Lee. Bipedal gait recharacterization and walking encoding generalization for stable dynamic walking. In *2016 IEEE International Conference on Robotics and Automation (ICRA)*, pages 1788–1793. IEEE, 2016.
- [66] Yan Gu, Bin Yao, and CS George Lee. Time-dependent orbital stabilization of underactuated bipedal walking. In *2017 American Control Conference (ACC)*, pages 4858–4863. IEEE, 2017.

- [67] Shuuji Kajita and Kazuo Tani. Study of dynamic biped locomotion on rugged terrain-theory and basic experiment. In *Advanced Robotics, 1991. 'Robots in Unstructured Environments', 91 ICAR., Fifth International Conference on*, pages 741–746. IEEE, 1991.
- [68] Jerry E Pratt and Russ Tedrake. Velocity-based stability margins for fast bipedal walking. In *Fast Motions in Biomechanics and Robotics*, pages 299–324. Springer, 2006.
- [69] Hongkai Dai and Russ Tedrake. Planning robust walking motion on uneven terrain via convex optimization. In *Humanoid Robots (Humanoids), 2016 IEEE-RAS 16th International Conference on*, pages 579–586. IEEE, 2016.
- [70] Andreas Hofmann, Marko Popovic, and Hugh Herr. Exploiting angular momentum to enhance bipedal center-of-mass control. In *2009 IEEE International Conference on Robotics and Automation*, pages 4423–4429. IEEE, 2009.
- [71] Ambarish Goswami and Vinutha Kallem. Rate of change of angular momentum and balance maintenance of biped robots. In *IEEE International Conference on Robotics and Automation, 2004. Proceedings. ICRA'04, 2004*, volume 4, pages 3785–3790. IEEE, 2004.
- [72] Xiaobin Xiong and Aaron Ames. Sequential motion planning for bipedal somersault via flywheel slip and momentum transmission with task space control. *arXiv preprint arXiv:2008.02432*, 2020.
- [73] Jessy W Grizzle and Christine Chevallereau. Virtual constraints and hybrid zero dynamics for realizing underactuated bipedal locomotion. In Bruno Siciliano and Oussama Khatib, editors, *Springer handbook of robotics*. Springer, 2016.
- [74] Benjamin Morris and Jessy W Grizzle. Hybrid invariant manifolds in systems with impulse effects with application to periodic locomotion in bipedal robots. *IEEE Transactions on Automatic Control*, 54(8):1751–1764, 2009.
- [75] Ching-Long Shih, Jessy Grizzle, and Christine Chevallereau. From stable walking to steering of a 3d bipedal robot with passive point feet. *Robotica*, 30(7):1119–1130, 2012.
- [76] William Yang and Michael Posa. Impact invariant control with applications to bipedal locomotion. *arXiv preprint arXiv:2103.06907*, 2021.
- [77] S. Kajita and K. Tani. Study of dynamic biped locomotion on rugged terrain-derivation and application of the linear inverted pendulum mode. In *Robotics and Automation, 1991. Proceedings., 1991 IEEE International Conference on*, pages 1405–1411 vol.2, 1991.
- [78] Matthew J Powell, Ayonga Hereid, and Aaron D Ames. Speed regulation in 3D robotic walking through motion transitions between human-inspired partial hybrid zero dynamics. In *Robotics and Automation (ICRA), 2013 IEEE International Conference on*, pages 4803–4810. IEEE, 2013.
- [79] S. Kajita, T. Yamaura, and A. Kobayashi. Dynamic walking control of biped robot along a potential energy conserving orbit. *IEEE Transactions on Robotics and Automation*, 8(4):431–437, August 1992.
- [80] Eric R Westervelt, Christine Chevallereau, Jun Ho Choi, Benjamin Morris, and Jessy W Grizzle. *Feedback control of dynamic bipedal robot locomotion*. CRC press, 2007.
- [81] Hereid Ayonga. Fast Robot Optimization and Simulation Toolkit(FROST). <https://ayonga.github.io/frost-dev/>.
- [82] Ross Hartley, Maani Ghaffari, Ryan M Eustice, and Jessy W Grizzle. Contact-aided invariant extended kalman filtering for robot state estimation. *The International Journal of Robotics Research*, 39(4):402–430, 2020.
- [83] Ross Hartley. Invariant-EKF. <https://github.com/RossHartley/invariant-ekf>.
- [84] K. Galloway, K. Sreenath, A. D. Ames, and J. W. Grizzle. Torque saturation in bipedal robotic walking through control lyapunov function-based quadratic programs. *IEEE Access*, 3:323–332, 2015.
- [85] E. R. Westervelt, G. Buche, and J. W. Grizzle. Experimental validation of a framework for the design of controllers that induce stable walking in planar bipeds. *International Journal of Robotics Research*, 24(6):559–582, June 2004.
- [86] Experiment Video Compilation. <https://youtu.be/o8msaembEu8>.
- [87] Michigan Robotics: Dynamic Legged Locomotion Lab Youtube Channel. <https://www.youtube.com/channel/UCMfDV8rkQqWhUwnTAYaQ0tQ>. Accessed: 2021-05-09.
- [88] Christian Ott. *Cartesian impedance control of redundant and flexible-joint robots*. Springer, 2008.